LMU LUDWIG-MAXIMILIANS-UNIVERSITÄT MÜNCHEN

Studies of an Electrically Conducting Organic Material: Tetrathiafulvalene-7,7,8,8-Tetracyanoquinodimethane

Frida Lindberg

LUND UNIVERSITY

MASTER THESIS
by due permission of the Faculty of Engineering, Lund University, Sweden.

To be defended at k-space, Sölvegatan 14, Lund, Sweden. Date 19th June 2014 and time 10:00.

Opponent

Linnéa Jonsson

Organization
LUND UNIVERSITY
LUDWIG-MAXIMILIANS UNIVERISTÄT
Author: Frida Lindberg

Document name
Master Thesis
Date of issue 2014-10-08
Sponsoring organization

Title and subtitle

Studies of an electrically conducting material: Tetrathiafulvalene-7,7,8,8-Tetracyanoquinodimethane

Abstract

This thesis aims to investigate the electrical properties of the organic charge transfer complex Tetrathiafulvalene-7,7,8,8-Tetracyanoquinodimethane, TTF-TCNQ. This is done through two different experimental techniques: Hall characterization and terahertz measurements. Before performing the experiments, suitable devices for these techniques were designed and produced. The layer of TTF-TCNQ was evaporated by physical vapour deposition on an insulating contact of parylene-N and on metallic chromium. According to these results the most promising layer sequence is TTF-TCNQ deposited on top of parylene-N. The adhesive skills of TTF-TCNQ deposited on different materials was also tested using the standardized adhesion test ASTM D3359-97. Two types of electrical devices were produced, Hall devices and terahertz devices. A third sample was also produced in order to image the material of interest using a scanning electron microscope and to measure the film thickness of the polycrystalline TTF-TCNQ layer and of parylene-N.

The electric measurements provided the charge carrier concentrations, the sheet carrier density and the conductivity of TTF-TCNQ. The charge carrier densities were high but the measured conductivity was very low. This indicates that the measurement techniques used here may not be very suitable for the both hole and electron conducting TTF-TCNQ material, as the effect of the oppositely charged charge carriers cancel each other out. Also, polycrystalline TTF-TCNQ, which was used here, seems to have a much lower mobility than single crystalline TTF-TCNQ. When working with the type of one-dimensional conductivity observed in TTF-TCNQ it is therefore important to grow single crystalline TTF-TCNQ when very high conductivities are desired.

The thesis provides an idea of charge carrier transport in molecular materials, electrical measurement techniques and how to produce a suitable device for examining TTF-TCNQ using terahertz measurements and Hall characterization.

Key words

Supplementary bibliographical information

Language: English

ISSN and key title

ISBN

Recipient's notes

Number of pages

Price

Security classification

Signature _____Date 2014-10-08_

LMU LUDWIG-MAXIMILIANS-UNIVERSITÄT MÜNCHEN

Studies of an Electrically Conducting Organic Material: Tetrathiafulvalene-7,7,8,8-Tetracyanoquinodimethane

Frida Lindberg

LUND UNIVERSITY

Divison of Solid State Physics
Department of Physics
Lund University
Sweden

in cooperation with

Lehrstuhl für Photonik und Optoelektronik
Department für Physik und CeNS
Ludwig-Maximilians Universität
Deutschland

Faculty of Engineering
Depratment of Physics
Division of Solid State Physics

Printed in Sweden by Media-Tryck, Lund University
Lund 2014

Preface with Acknowledgements

This work was performed from January 2014 to June 2014, as a master thesis project for the engineering program Technical Nanoscience at Lunds Tekniska Högskola, LTH, in Lund, Sweden. The project was conducted at the terahertz group at Ludwig-Maximilians Universität, LMU, in Munich, Germany. The main focus of this thesis is on the quasi-one-dimensional organic charge transfer metal TTF-TCNQ, combining research within chemistry, material science, electronics and physics.

I want to thank Professor Kersting at Ludwig-Maximilians Univeristät and Associate Professor Dan Hessman at Lunds Tekniska Högskola for their supervision during this project and Markus Prinz for introducing me to the machines and cleaning procedures. I also want to thank Stefan Engelbrecht for his valuble input, patience and aid throughout the project. Thank you to Jaekwon Do for helping me with the SEM and many thanks to Johan Ekström for helping me to create the 3D images in this thesis report, using Blender. Thank you Thomas Ahrend for all the hard work fixing wiring and broken equipment and thank you Christopher Hackl for the highly appreciated encouragement.

I want to thank Associate Professor Dan Hessman again for his highly appreciated and valuable feedback on this thesis.

Finally, I also want to thank my family for their immense support and love as well as endurance and tolerance throughout my five years of nanotechnology engineering studies. I want to give special thanks to my dear love Casper, who has been by my side for 14 years helping me overcome all difficulties and without whom none of this would have been possible.

Contents

1. Introduction

1.1 The terahertz group

The terahertz group is a research group in the department of photonics and optoelectronics at Ludwig-Maximilian's Universität in Munich, Germany. The main research interest of the group lays in examining the electrical properties of different materials using terahertz spectroscopy. The ongoing research is focused on organic materials and electronics.

1.2 Background

Inorganic metals are non-biodegradable and can be recycled any number of times without losing their properties. However, metals are also non-renewable, limiting the amount of these materials available. As the economy of developing countries increase, the demand for metallic materials increase. Yet, decreasing the amount of material required in process and minimizing production spillage, will still not provide a sufficient amount of metals required to fulfil future demands [1].

The waste from inorganic metals cannot degrade, but instead accumulates in soils, waters and in the biosphere. This build-up of metals causes a disturbance in the ecosystems and may lead to metal poisoning [2]. It is therefore not only important to investigate bio-degradable and renewable metallic materials from an economical perspective, but also from an ecological perspective.

Carbon and hydrogen are among the most common elements on earth [3]. Many materials consisting of mainly carbon and hydrogen are both bio-degradable and inexpensive. Replacing inorganic materials with organic materials would result in immense cost reductions and reduce environmental impacts. One such organic conductor is tetrathiafulvalene-7,7,8,8-tetracyanoquinodimethane, TTF-TCNQ. TTF-TCNQ is a charge transfer complex that obtains high electrical conductivity in one dimension. It is cheap and has low toxicity, making it highly interesting for biological devices and organic electronics [4, 5]. For instance, transistors require charge injections

from electrodes into the semiconductor. Today, the electrodes mainly consist of inorganic materials such as Au or Ag. If the semiconductor is an organic material, the inorganic-organic interface produces a poor contact with large differences in work functions, lowering the overall device performance [4]. Instead, TTF-TCNQ can be used as an electrode, creating a better interface and contact, and a more efficient charge carrier injection, improving the device performance. As TTF-TCNQ is both electron and hole conducting, it can be used as an electrode for both n-type and p-type transistors.

Another application for TTF-TCNQ is as a repairing agent in electronic circuits. TTF and TCNQ form the charge transfer complex TTF-TCNQ by simple contact. Therefore, as a device breaks due to mechanical stress, TTF and TCNQ can be transported in microcapsules to the area of damage. Once at the desired location, the microcapsules are ruptured and TTF and TCNQ can form TTF-TCNQ, restoring conductivity in the damaged area [6].

1.3 Purpose of the Study

Due to the benefits of replacing inorganic materials with organic materials, TTF-TCNQ has been investigated as an electrical conductor in this thesis. The aim of this thesis is to examine the electric properties of TTF-TCNQ through terahertz measurements, which has not previously been performed on TTF-TCQ, and Hall characterization. In order to do so, different devices must be produced and a suitable design for these must be determined. Due to the techniques, the devices used for examining TTF-TCNQ must have certain designs. To find an appropriate device with a smooth, well ordered TTF-TCNQ layer, TTF-TCNQ will be deposited on different substrates. The adhesion strength and surface structure on the different substrates will be tested and the results will be used to design the devices. Following this, the devices will be produced and the electronic measurements mentioned will be performed.

The results obtained from this project will determine whether or not there might be suitable applications of TTF-TCNQ in the current research ongoing at the terahertz group.

1.4 Disposition

This thesis has been divided into five main chapters following the introduction. The first chapter introduces the theoretical background to charge carrier motion in atoms, molecules and molecular systems followed by an introduction to the main material of interest, TTF-TCNQ. The second chapter describes how the electric devices were designed and produced for the measurement techniques used later on. The final two chapters describe the two electric techniques used in this project, Hall characterization and terahertz measurements as well as the results obtained during these experiments.

2. Theory

2.1 Electrical conductivity in materials

Electric currents consist of charge flows. How easy a current can flow in a material depends on several different factors. One of the main factors affecting carrier flow is the atomic structure of the material.

2.1.1 The probability wave

In quantum mechanics, charge carriers are described by probability waves. The carriers are affected by present potentials, limiting their trajectory path. The wave functions, ψ, for the carriers are described by the Schrödinger equation, which takes into consideration the impact of potentials, $V(\bar{r})$:

$$-\frac{\hbar^2}{2m}\nabla^2\psi(\bar{r}) + V(\bar{r})\psi(\bar{r}) = E\psi(\bar{r})$$

Equation 1.

Equation 1 describes the time-independent Schrödinger equation in three dimensions, where $\hbar$ is Planck's constant, $\nabla^2 = \frac{\partial^2}{\partial x^2} + \frac{\partial^2}{\partial y^2} + \frac{\partial^2}{\partial z^2}$, m is the particle's mass and E is the energy of the particle. This equation can be used to find the atomic orbitals and energies of the charge carriers around the atomic nucleus if $V(\bar{r})$ describe the atomic potential [7].

2.1.2 Atomic orbitals

In an atom the electrons are all bound to the positively charged nucleus, i.e., the electron is affected by a potential creating a well, confining the charge carriers. A simplified picture can be obtained by assuming the electron to be considered as a free particle inside an infinitely deep square well (see Figure 1) and solving the Schrödinger equation.

At the barriers of the system the potential is infinitely high and the probability of finding the electron there is zero and the wave function must also be zero. The boundary conditions for a potential well of size a are thus, ψ (x = 0) = 0 and ψ(x = a) = 0. The waves travel back and forth inside the system, creating standing waves between the potential barriers. However, most waves are cancelled out due to destructive interference. This will result in only certain allowed energy states in the system. Thenceforth, the charge carriers surrounding an atom all reside in stationary energy states.

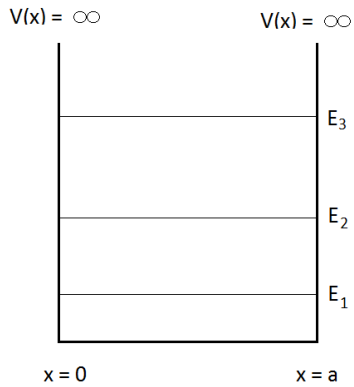

Figure 1. The quantum well schematically shows an atomic system. The positively charged nucleus confines a negatively charged electron in a finite space. The quantum well above shows the three lowest stationary energy levels at which the electron may reside.

Figure 1 shows an image of the stationary energy states in an infinite quantum well. Each energy state is labelled by a number, 1, 2, 3.. etc., called the quantum number, *n*. The wave functions at these energy states are called orbitals. As each element has a set amount of electrons surrounding its nucleus, it also has a set number of occupied atomic orbitals. A consequence of quantum mechanics, is that two electrons cannot have the same quantum number. However, electrons are fermions and can have opposite spin. Each energy state can retain up to two electrons assuming they are of opposite spin. To ensure a total energy as low as possible, the electrons will reside at the lowest possible energy levels, gradually occupying higher energy states, two by two [7].

In atoms, there are different types of orbitals within the energy levels: s-orbitals, p-orbitals, d-orbital, f-orbitals etc. The shape of these orbitals varies and so does the number of possible electron states. In three dimensions the s-orbitals are spherical, whereas the p-orbitals are elongated in each direction as

shown in Figure 2. Since the s-orbitals are spherical, each quantum number only creates two possible electron states at a given energy level. As the p-orbitals are directed in different dimensions, each quantum number (and so also each energy level) allows for three p-orbitals: p_x, p_y and p_z. Therefore, there are in total 6 possible states for the electrons to occupy in a p-orbital [8].

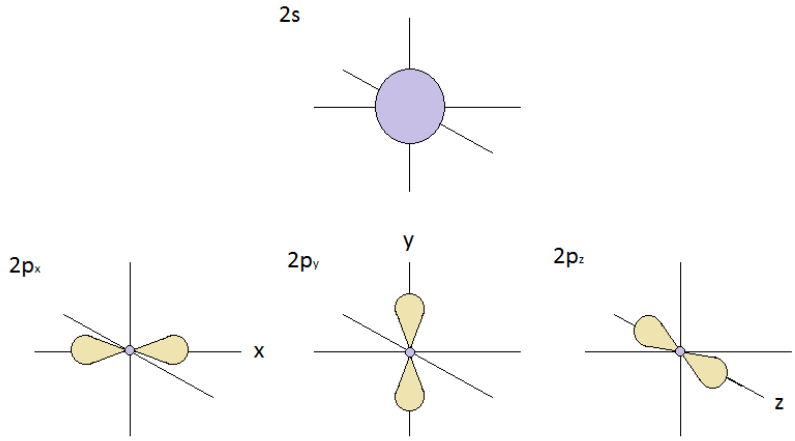

Figure 2. Graphical description of the atomic s- and p-orbitals. The s-orbitals are spherically shaped whereas the p-orbitals are directed along each axis.

2.1.3 Molecular orbitals

Molecules consist of several atoms bound together. When two atoms bind together their atomic orbitals interact and create molecular orbitals [10]. The spherical nature of s-orbitals allows them to create bonds in any direction. The same does not apply for p-orbitals. As p-orbitals are directed along an axis, these orbitals can only create bonds in certain directions. If the binding occurs along the axis direction of the p-orbital a σ-bond arises. If instead the binding occurs between two parallel p-orbitals a π-bond arises. The different types of bonds are shown in Figure 3 [8].

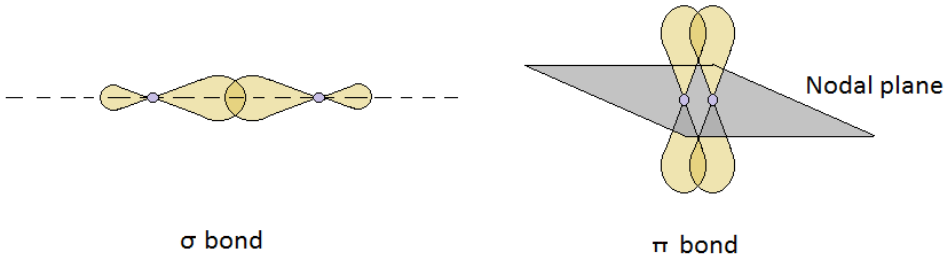

Figure 3. Two atomic p-orbitals interact and create molecular orbitals. Depending on the direction of the interaction, either σ-bonds or π-bonds are formed.

The electrons closest to the nucleus are all tightly bound. Hence, these electrons do not take part of reactions or bonding, only the weakest bound electrons do. These electrons belong to the highest occupied atomic orbitals and are called valence electrons [10].

In addition to creating bonds, the atomic interaction also causes the atomic energy levels to split. The number of orbitals must be conserved, hence two atomic orbitals will create two molecular orbitals, above and below the original energy level, corresponding to the antibonding and bonding orbital respectively. The electrons first occupy the lower energy level, lowering the total energy of the molecule as compared to the two individual atomic systems, binding the two atoms together. The strength of the bond increases with an increasing overlap. The highest occupied molecular orbital is abbreviated as HOMO and the lowest unoccupied molecular orbital is abbreviated as LUMO. As molecules interact, so will their molecular orbitals and energy levels, causing them to split. A higher number of interacting molecules increases the energy level splitting. Eventually, the number of energy levels lay so close to each other that the levels are instead considered as bands [8, 9, 11].

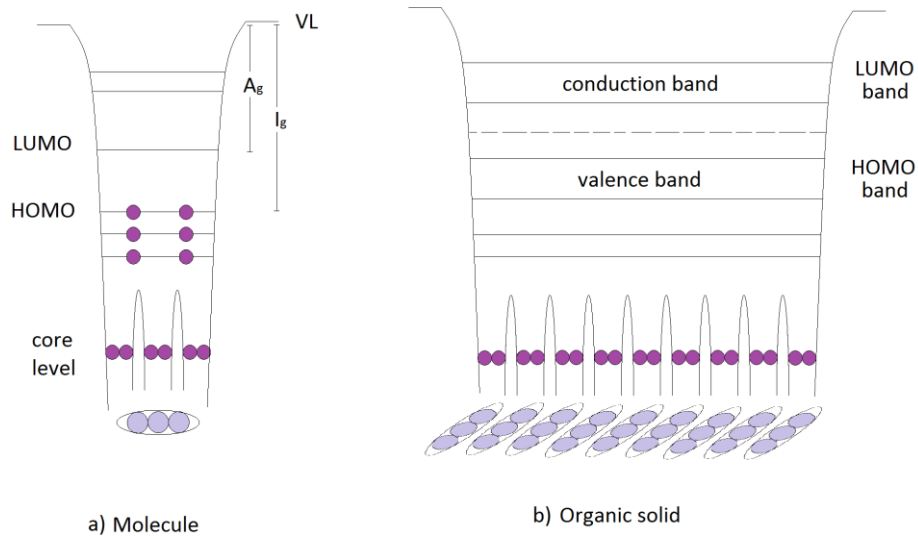

Figure 4. In a) three atoms interact and create a molecule. The atomic orbital interaction gives rise to new molecular orbitals. HOMO represents the highest occupied molecular orbital while LUMO represents the lowest unoccupied molecular orbital. VL denotes the vacuum level, I_g the ionization energy and A_g the electron affinity. In b) multiple molecules interact to form a solid, this intermolecular interaction gives rise to bands.

Figure 4 shows the formation of molecular orbitals as three atomic orbitals interact in image a). Each atom contains its orbitals due to the electron-nucleus attraction. As the atoms come together their atomic orbitals interact, creating new molecular orbitals, containing the HOMO and LUMO levels. VL in Figure 4 represents the vacuum level. The distance between HOMO and VL is called the molecule's ionization energy, I_g. The distance between LUMO and VL is called the molecule's electron affinity, A_g. Image b) in Figure 4 shows the formation of intermolecular bands as the three-atomic molecules interact with each other, creating a solid material. The interaction causes further energy level splitting, eventually leading to the formation of the energy bands. The weaker the interaction, the more narrow the intermolecular bands are as the charge carriers are more localized in each molecule. As the molecular overlap increases, the energy bands broaden, increasing the charge carrier delocalization [12].

2.1.4 Tetrathiafulvalene-7,7,8,8-Tetracyanoquinodimetahne, TTF-TCNQ

The material of interest in this thesis is Tetrathiafulvalene-7,7,8,8-Tetracyanoquinodimetahne, TTF-TCNQ. Therefore, this molecular complex is further described in the sections below.

2.1.4.2 Crystal structure

In ordered materials, the atomic or molecular arrangements are described by the crystal structure. Each crystal consists of repeating identical blocks. These blocks, or unit cells, are described by three lattice constants. The lattice constants provide information about the size of the unit cells in each direction. To fully describe the unit cell, the angles between the three different lattice constants must also be known [13]. If the size of the unit cells are very different between two materials deposited on top of each other, an energy costing lattice strain occurs at the interface. This unables the formation of a smooth surface [14]. There are several different forms of unit cells, such as, cubic, hexagonal, monoclinic etc. [10]. Figure 5 below shows the lattice parameters of a monoclinic unit cell.

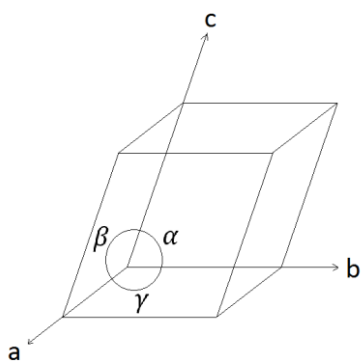

Figure 5. A monoclinic unit cell showing the lattice parameters defining the crystal structure.

The molecular structure of TTF (Tetrathiafulvalene) and TCNQ (7,7,8,8-Tetracyanoquinodimethane) can be seen in Figure 6.

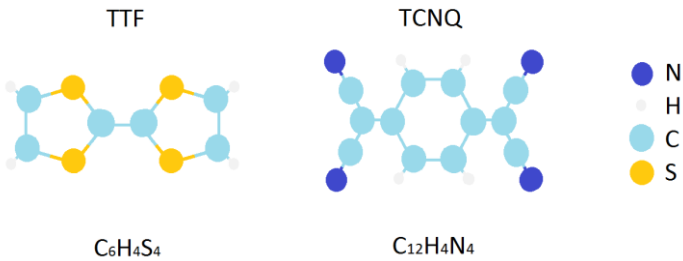

Figure 6. Molecular structure of TTF and TCNQ.

The TTF-TCNQ complex crystallizes in a monoclinic crystal structure comprised of segregated, columnar stacks along the b-direction of the unit cell. Each stack consists of either TTF or TCNQ molecules. The crystal structure is shown in Figure 7 as seen from the b-direction and the a-direction of the unit cell. The lattice dimensions of the monoclinic unit cell are $a = 12.298\ Å, b = 3.819\ Å, c = 18.468\ Å, \alpha = \gamma = 90°$ and $\beta = 104.46°$ [15].

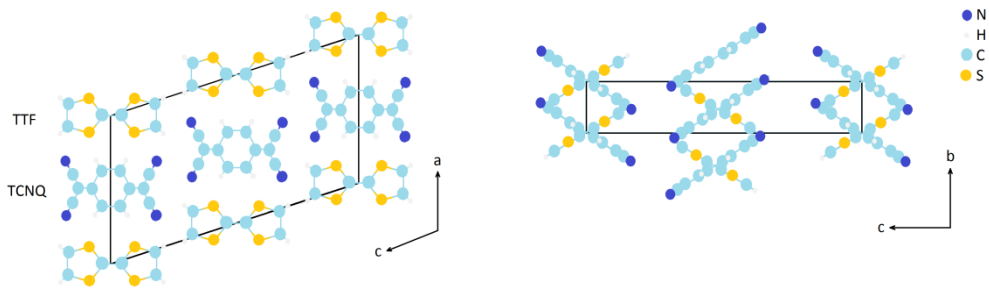

Figure 7. Crystal structure of TTF-TCNQ showing the columnar stacks of alternating TTF and TCNQ. The left image shows the crystal structure as seen from the b-direction of the unit cell and shows how the segregated stacks of TTF and TCNQ alter along the a-direction. The right image shows the crystal structure as seen from the a-direction of the unit cell and shows how each stack is comprised of either TTF or TCNQ molecules laying on top of each other in the b-direction.

2.1.4.1 Charge transfer complex

If a molecule with a high electron affinity, called an acceptor, interacts with a molecule with low ionization energy, called a donor, a charge transfer can arise between the HOMO of the donor and the LUMO of the acceptor. Two such molecules are TTF and TCNQ. The energy difference between the HOMO in TTF and the LUMO in TCNQ is low (≈ 0.80 eV), enabling TTF to donate an

electron to TCNQ [16]. The HOMO and LUMO bands of TTF and TCNQ can be seen in Figure 8.

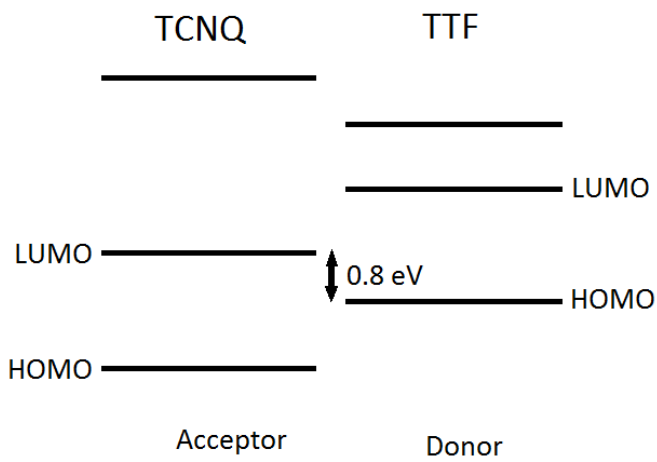

Figure 8. The energy bands of TTF and TCNQ showing the HOMO and LUMO bands in each molecule relative each other.

This charge transfer complex is called TTF-TCNQ. As TTF donates an electron to TCNQ an excess amount of holes arises in TTF and an excess amount of electrons arises in TCNQ. The interacting orbitals within the TTF stacks and the TCNQ stacks are both π-orbitals and create a directed charge transfer along one direction, creating channels allowing electric conduction in one dimension. The π- π-interaction can be seen in Figure 9. Due to the excess amount of holes in TTF these stacks are hole conducting along the π-orbital overlap, while the TCNQ stacks are electron conducting along the π-orbital overlap [15].

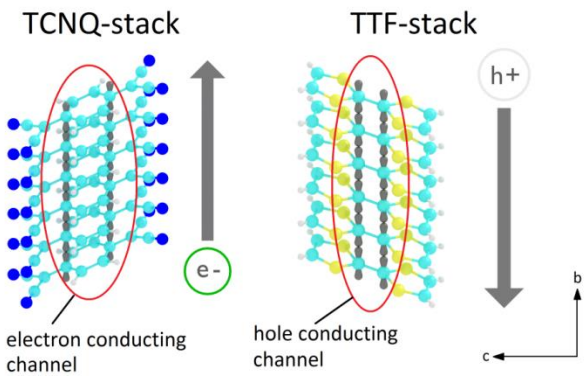

Figure 9. The charge transfer between TTF and TCNQ gives rise to an electron- and hole channel in TCNQ and TTF respectively, along the stacking direction due to the π-orbital interactions between molecules. This image shows both a TCNQ stack and a TTF stack as seen from the a-direction in the crystal structure.

2.1.4.3 Conductivity

The conductivity, σ, of a material is a measure of how easy a current can flow through it, i.e. how easy charge carriers can flow. The conductivity of TTF-TCNQ depends on the material's crystal structure which in turn depends on the orbital interactions between TTF and TCNQ. As seen in Figure 9, both the TTF and TCNQ stacks are conducting, TTF is hole conducting and TCNQ is electron conducting along the short b-axis. The weak interactions and large distances in the other two directions creates a highly anisotropic conductivity, where $\sigma_b > \sigma_c > \sigma_a$ [17]. The conductivity along the b-axis, which is where the π-π-overlap occurs, is around 500 S/cm at room temperature [8].

Studies show that the number of defects in TTF-TCNQ plays an important role in the conductive properties of the material [18]. Structural disorder induced by irradiation causing lattice defects show that a higher defect concentration lowers the conductivity. The conductivity decreases due to the disruption of a long range order in TTF-TCNQ as defects block the charge transfer along the chains.

The main contribution to electric currents in an ideally structured TTF-TCNQ is the charge transport along delocalized states in the created electron and hole channels. However, there is also another mechanism contributing to the conductivity. This mechanism is called hopping, as charge carriers "hop" between molecule chains. The importance of the hopping mechanism on the conductivity of a material increases as the structural order decreases. Hopping occurs between localized energy states and requires absorption or emission of phonons, corresponding to the energy difference between the states. The probability of this tunneling transition depends on both the temperature and the distance between localized states. A shorter distance between states requires a lower transition energy and a higher temperature increases the phonon-electron interactions and thus increases the hopping rate [8].

2.1.6 Electric currents

For a net current to flow through a material, an electric field must be applied, accelerating the charge carriers. A higher field causes a higher current as it increases the electron drift velocity. The current density is as the current, I, per unit area, A, and can be described as:

$$J = \frac{I}{A} = \sigma E$$

Equation 2.

where E, is the electric field and σ, is the conductivity of the material. The relation between the conductivity and charge carrier concentration, n_{3D}, of a material is defined as:

$$\sigma = \frac{q n_{3D} v}{E}$$

Equation 3.

where q is the elementary charge and v is the drift velocity of the charge carriers. Another important material constant is the mobility, μ. The mobility is a proportionality constant that relates the drift velocity to the applied electric field:

$$v = \mu E$$

Equation 4.

Equation 3 and 4 give a relation between the conductivity and the mobility [19]:

$$\sigma = q n_{3D} \mu$$

Equation 5.

thus, a larger mobility or charge carrier concentration provides a higher conductivity.

3. Device design and production

The main aim of this thesis is to examine the electrical properties of TTF-TCNQ using two different measurement techniques, terahertz characterization and Hall characterization. Before these measurements could be performed devices had to be designed and produced. The first part of this chapter is therefore devoted to device design while the second part of this chapter is devoted to device production.

3.1 Device design

The design of the devices was determined by first examining the adhesion strength and surface structure of TTF-TCNQ on different types of underlying substrates. Terahertz devices require the material to be embedded between two metal contacts and an insulator so a bias can be applied over it. There are two different layer sequences possible, depending on if the insulator or TTF-TCNQ is deposited first, see Figure 10.

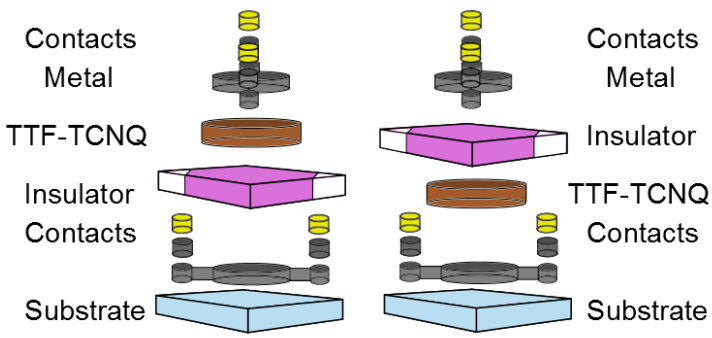

Figure 10. Two types of device designs for terahertz spectroscopy, showing the possible layer sequence. In the left image, the insulator is deposited before the TTF-TCNQ layer. In the right image the TTF-TCNQ layer is deposited before the insulator.

The structure of a Hall device can be seen in Figure 11.

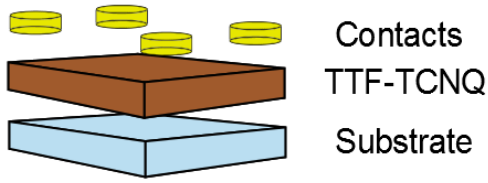

Figure 11. Layer sequence for the device for Hall characterization.

The choice of materials for the devices used in this project are mainly based on the experience of previous research groups. Parylene-N is used as an insulator because it has a low water permeability and forms a completely homogeneous, pin-hole free coating [20]. It is important that the absorption of radiation is minimized in the insulating layer and metal contacts of a terahertz device in order to measure the transmission signal through the layer of interest. The refractive index, n, of a material is a complex number if radiation is absorbed, thus the imaginary part, $\mathrm{Im}(n)$, is given by the absorption. The absorption of radiation with a wavelength λ, in a material with the refractive index n, is described by the absorption coefficient, α [21].

$$\alpha = \frac{4\pi Im(n)}{\lambda}$$

Equation 6.

In this project sapphire substrates are used for the terahertz devices instead of e.g., glass, as sapphire has a lower refractive index and glass is absorbing at terahertz frequencies. Hall characterization is not an optical technique and hence, does not require any concern regarding minimizing of light absorption. Therefore, the material of interest can be deposited on e.g., glass, instead of sapphire.

Further, there are several ways to create thin films of various materials, the methods used in this project are chemical vapour deposition, CVD, and physical vapour deposition, PVD. The major difference between the two deposition techniques is the chemical reaction undergone in CVD, whereas the PVD technique simply transforms the material to be deposited from one form to another.

3.1.1 Chemical vapour deposition, CVD

The general chemical route undergone in a CVD process can be written as:

$$A(g) + B(g) \rightarrow C(s) + D(g)$$

Equation 7.

where A and B are the reactants (in gas phase), C is the deposited material and D is a gaseous product. The reactants are transferred into the deposition chamber and diffuse to the surface of the substrate were they adsorb and undergo a chemical reaction. This may be followed by surface migration and lattice incorporation. Any remaining products from the chemical reaction then desorb and diffuse away from the substrate before being pumped out from the chamber.

The main components of the parylene-N CVD apparatus are the sublimation furnace, the pyrolysis furnace, the vacuum pump and the deposition chamber (see Figure 12). The vacuum system is connected to a cold trap to prevent excessive parylene-N monomers and other by-products from contaminating the pump. The samples must be kept in vacuum pressure to prevent oxygen molecules from being incorporated into the deposited film [22]. Figure 12 shows a schematic image of a parylene-N CVD process. Parylene-N powder is loaded in a boat which is inserted into the sublimation chamber. The parylene-N sublimes from solid phase to gas phase at temperatures, T, above 70 ℃. Therefore, the sublimation chamber is heated to $T = 120$ ℃ producing a gas of parylene-N dimers. The parylene-N dimers are cleaved into two monomers above 550 ℃, hence, the pyrolysis furnace is heated to 600 ℃. The sample holder in the deposition chamber is situated on top of a Peltier element that transfers thermal energy away from the substrate holder. The substrate holder is cooled to around 10 ℃ and thus, once the monomer gas reaches the deposition chamber, parylene-N can be deposited onto the cool samples, adsorb and polymerize.

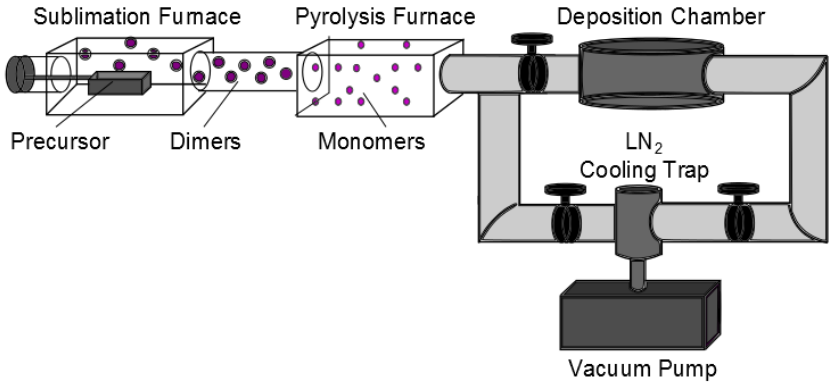

Figure 12. Schematic image of a parylene-N CVD process. The parylene-N is loaded in a boat and inserted into the sublimation furnace where it is heated until a gas of parylene-N dimers is created. The parylene-N dimers travel to the pyrolysis furnace and are cleaved into monomers. Once the monomers reach the cool samples they adsorb and polymerize.

All tubes used in the CVD to connect the different pieces are heated above the sublimation temperature to prevent contamination. The figure below describes the polymerization route of parylene-N:

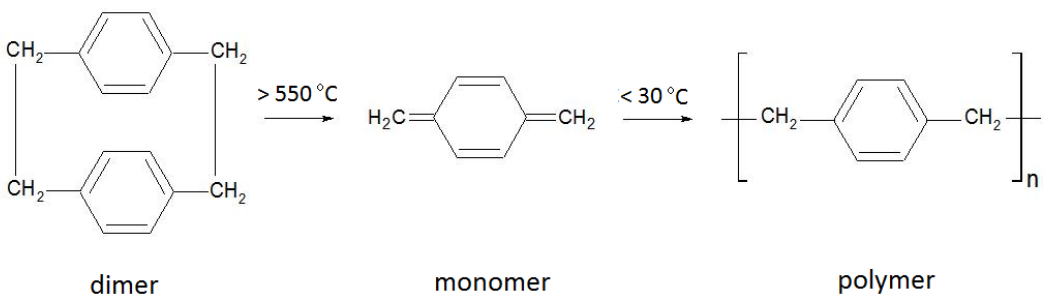

Figure 13. Polymerisation route for parylene-N. The parylene-N dimers are cleaved into monomers whereafter they can polymerize and create a film.

Parylene in general has poor adhesive strength to its underlying substrate. This strength may be increased by using e.g., silane A174 as a contacting agent between organic and inorganic materials [22].

3.1.2 Physical vapour deposition, PVD

As previously mentioned, the PVD process transforms the material to be deposited from one form to another. There are several different types of PVD processes such as: vacuum deposition, sputter evaporation, ion plating etc. The method used in this project is vacuum deposition, therefore, this will be the main focus in this section.

The physical vacuum deposition process takes place in a low pressure (vacuum) environment at around 10^{-5} – 10^{-9} mbar[23]. The mean free path for N_2 and O_2 molecules at room temperature can be related to the pressure as [24]:

$$\lambda(cm) \approx \frac{0.007}{P(mbar)}$$

Equation 8.

Consequently, a liquid or solid source that is heated so it vapourizes will travel towards the substrates in a straight line without colliding with gas molecules due to the large mean free path (>5 m) obtained in the vacuum environment. This also enables the use of a mask for patterned deposition. Once the vapourized material reaches the substrate it condenses and forms a thin film. To increase the deposition rate the substrates and material source are kept close to each other, but far enough to prevent heating of the samples due to heat radiation from the source. As a material is heated, the first vapourized particles are impurities and contaminants. Hence, before depositing a material by PVD the material is pre-heated below its evaporation temperature to allow any dirt to evaporate [24]. Figure 14 shows an image of a PVD set-up.

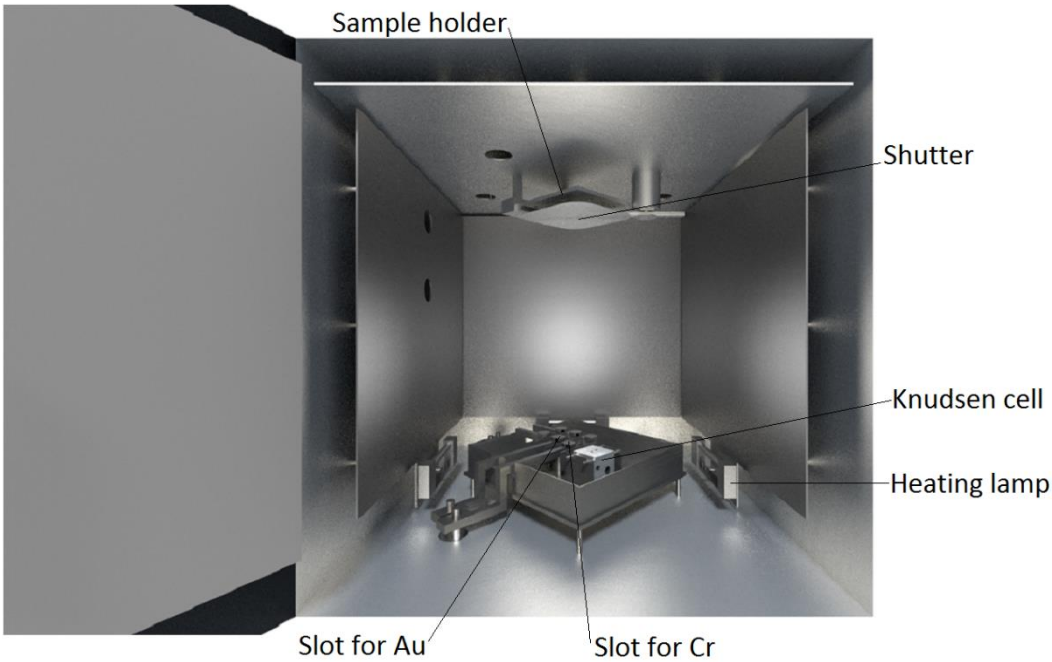

Figure 14. 3D image of the structure for the deposition chamber used for PVD.

The material to be deposited can be heated in several different ways, e.g., through resistive heating or by using a Knudsen cell. Resistively heated materials are heated electrically by applying a current through for instance, a rod or a boat [23, 25]. Here below follows a short description of a Knudsen cell.

A Knudsen cell is a container which is filled with the material to be deposited. Figure 25 shows a 3D image of a Knudsen cell. There are two smaller holes on one side of the cell for temperature sensors and one larger hole for a heating lamp to heat the cell. The top two holes are the material reservoir and the orifice through which the material evaporates, connected to each other by a channel. To deposit a uniform film layer, a large distance between the Knudsen cell and sample is desired. However, as mentioned this will decrease the deposition rate, and may also increases the probability of incorporating contaminants in the film [25].

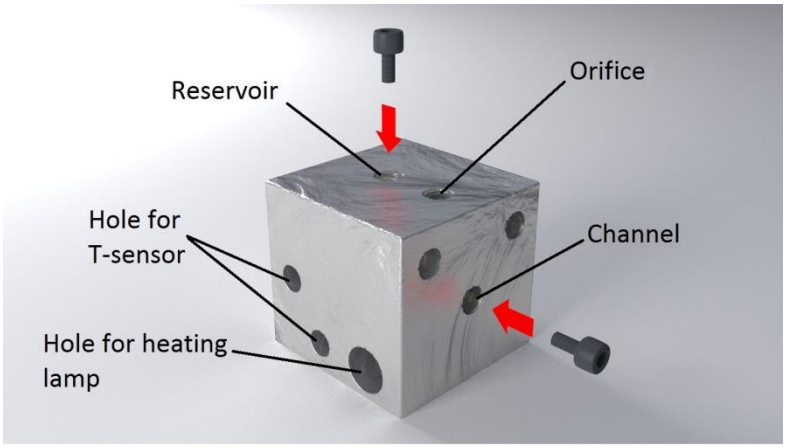

Figure 15. 3D image of the Knudsen cell used for PVD in this project, displaying its different parts and compartments.

To control the PVD process better a movable shutter is often used. The shutter is a shield preventing deposition on to the samples unless so desired. It can be used to avoid contamination during pre-heating, to control the time of deposition and to ensure deposition occurs only at a desired temperature or rate.

Quartz crystals are commonly used to measure the deposition rate and the film thickness during evaporation. The quartz crystal is piezoelectric, meaning that an applied voltage changes the volume of the crystal, causing the crystal to oscillate. As material evaporates onto the crystal, the oscillation frequency changes. The change in frequency is directly proportional to the mass deposited onto the crystal. The film thickness and deposition rate can therefore be obtained from the crystal movement [23].

3.1.3 Sample production

To design suitable electrical devices, three different model types were produced and examined. The structure of each model can be seen in Figure 16. Model A and B represent the two different layer sequences possible for terahertz devices and model C represents the Hall device. As only the surface properties and adhesion skills of the TTF-TCNQ were to be examined, the top layers were not deposited and neither were the contacts, as no electrical measurements were to be performed on these samples.

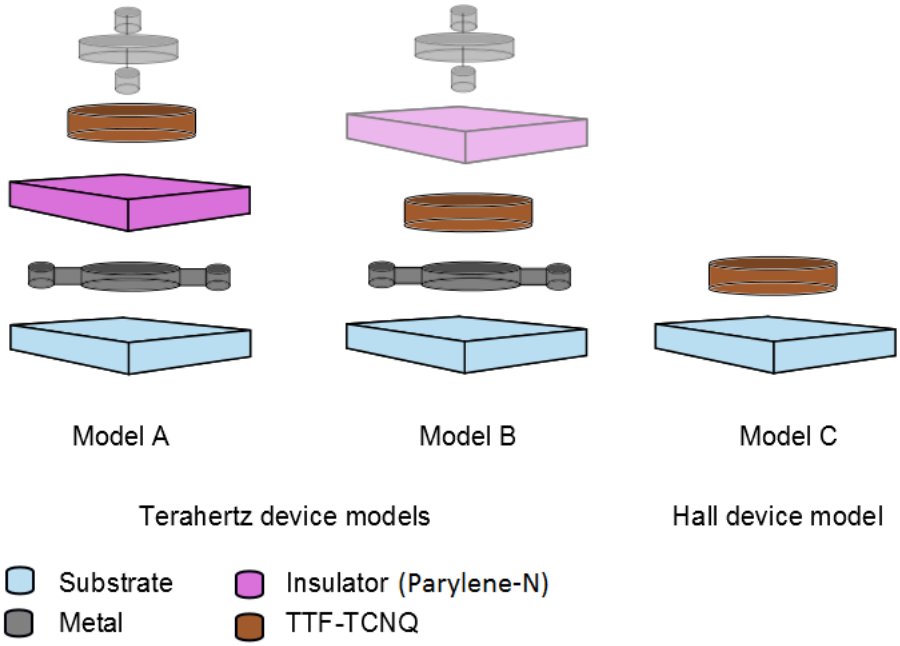

Figure 16. Devices produced for examining the adhesion skills and surface structure of TTF-TCNQ on different types of underlying substrates.

In total, three sets of each sample model A, B and C, where created. Table 1 summarizes the layer sequences for each sample produced.

Table 1. Materials used for different layers in different samples.

Name	A1	A2	A3	B1	B2	B3	C1	C2	C3
Model	A	A	A	B	B	B	C	C	C
Substrate	Sapphire	Sapphire	Sapphire	Sapphire	Sapphire	Sapphire	Glass	Glass	Glass
Insulator	Par-N	Par-N	Par-N	-	-	-	-	-	-
Metal	Cr	Cr	Cr	Cr	Cr	Cr	-	-	-
Contacts	-	-	-	-	-	-	-	-	-
TTF-TCNQ	Mask	Mask	No mask	Mask	Mask	No mask	Mask	Mask	No mask

All substrates were cleaned in a clean room according to the cleaning procedure described in Appendix A. To ensure that the samples were indeed clean, a laser test was performed. A green laser was mounted on a holder and the sample to be examined was held in the ray of light. If any spots or milky

coatings where observed, the sample was condemned dirty and hence, not used. After the cleaning process was performed, all model A and B samples were mounted in a PVD chamber together with a chromium rod. The pressure was pumped down whilst annealing the chamber, evaporating any O_2-molecules on the walls. After allowing the chamber to cool down, a 5 nm thick chromium layer was evaporated. Finally, all samples of model type A were deposited a 400 nm thick parylene-N layer through CVD.

Thereafter, a Knudsen cell was cleaned and filled with TTF-TCNQ. All samples were mounted in the PVD chamber together with the filled Knudsen cell. The pressure was pumped down whilst annealing the TTF-TCNQ, allowing dirt to evaporate. After annealing, a 150 nm thick TTF-TCNQ film was deposited, both through a mask and without a mask. The schematic images of model A-C in Figure 16 show the TTF-TCNQ film when a mask has been used. For the samples without a mask the TTF-TCNQ layer was deposited evenly all over the surface. All evaporation and process details can be found in Appendix B.

3.1.4 Surface structure

The surface of each model type was imaged with a scanning electron microscope. The images obtained can be seen in Figure 17.

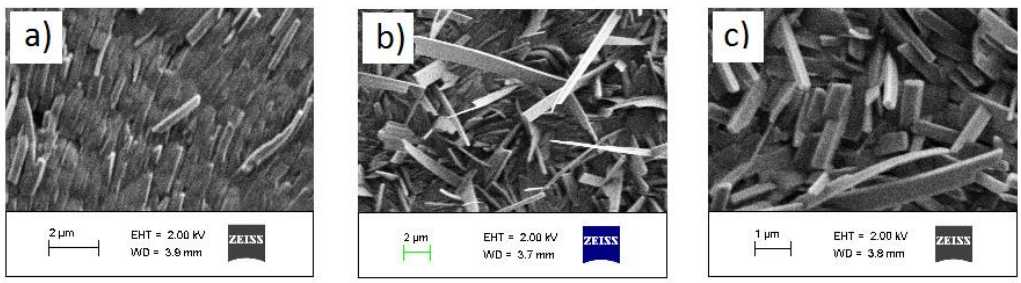

Figure 17. Scanning electron microscope images of model A, B and C (see figure 16), showing the surface structure on different substrates: a) parylene-N (model A), b) chromium (model B) and c) glass (model C).

Figure 17 a), shows model A, TTF-TCNQ deposited on parylene-N, Figure 17 b) shows model B, TTF-TCNQ deposited on chromium, and Figure 17 c) shows model C, TTF-TCNQ deposited on glass. All images show bar shaped TTF-TCNQ crystallites. Comparing the three images shows that parylene-N as an underlying substrate produces the most ordered, homogenous film. The TTF-TCNQ crystallites do not seem to organize in any preferred direction on

neither chromium nor glass. Instead, both underlying substrates create a very unorganized film. The charge carrier transport in TTF-TCNQ occurs along the ordered stacks of TTF and TCNQ [14]. Any disorder would therefore, lower the electric conduction. Due to this, the best model for the terahertz devices is model A instead of B as model A is more ordered.

As the glass substrate in model C produces such an unorganized TTF-TCNQ film, the Hall devices will as well be produced on parylene-N. The reason for why the surface structure on parylene-N is the most ordered is likely due to the high homogeneity of parylene-N. In comparison, glass is a very amorphous material [26], obviously creating an unorganized TTF-TCNQ film. TTF-TCNQ crystallizes in a monoclinic unit cell structure with lattice constants $a = 12.298\,\text{Å}, b = 3.819\,\text{Å}$ and $c = 18.468\,\text{Å}$ whereas chromium crystallizes in a body centred cubic unit cell with lattice constant $a = 2.89\,\text{Å}$ [27]. The large lattice mismatch causes high lattice strains, preventing the formation of a relaxed surface of TTF-TCNQ on chromium, which decreases the conductivity due to the lack of long range order. Henceforth, the most promising terahertz device model is model A. The Hall devices should also be produced with a parylene-N layer beneath the TTF-TCNQ film so a higher order can be obtained.

To further investigate the structure of TTF-TCNQ on parylene-N, the next appropriate procedure would be to create an x-ray diffraction pattern. From this, the crystallographic directions of the deposited film could be determined and related to the scanning electron microscope images, which may help in explaining the electric behaviour of the devices produced. However, due to lack of time, this was unfortunately not possible.

Before producing the electric devices, the adhesion strength of TTF-TCNQ on each underlying substrate was tested.

3.1.5 Adhesion strength

All sample models underwent the standardized adhesion test, ASTM D3359-97 [28] in order to determine which layer sequence produced the highest adhesion strength. Horizontal and vertical cuts were made, 1 mm apart, on the sample's surface using a scalpel, creating a checked pattern. A piece of Scotch tape was positioned on top of the cuts and pressure applied using a cotton swab to ensure full coverage. The tape was then pulled off in an 180° angle and the amount of TTF-TCNQ gone from the sample was examined. The adhesion strength of TTF-TCNQ was tested on three different underlying substrates, parylene-N (model A), chromium (model B) and glass (model C). The results

of TTF-TCNQ's adhesion on all these materials are summarized in Table 2 below.

Table 2. Results from the adhesion test performed on three different underlying substrates: parylene-N (A1-A3), chromium (B1-B3) and glass (C1-C3). The percentage shows the amount material gone.

Sample	Material gone	Mask
A1	100 %	Yes
A2	100 %	Yes
A3	100%	No
B1	50 %	Yes
B2	65 %	Yes
B3	65 %	No
C1	35 %	Yes
C2	25 %	Yes
C3	20 %	No

The adhesion of TTF-TCNQ on parylene-N in model A could not be determined as all the parylene-N was removed during the test. Therefore, Table 2 does not show the adhesion strength of TTF-TCNQ on parylene-N, but of parylene-N on chromium and sapphire. Parylene-N generally has poor adhesion skills to inorganic materials, hence, the results of the adhesion test in Table 2 were to be expected. Nevertheless, the adhesion skills of parylene-N can be enhanced by incorporating silane A174 in the film during the CVD process [22]. Also, all the TTF-TCNQ was removed along with the parylene-N, indicating that TTF-TCNQ adheres well to parylene-N.

Examining the results of the adhesion on chromium and glass confirms that TTF-TCNQ in general, adheres well to its substrate, the best adhesion being on glass. Due to the overall good results it is therefore, expected that the adherence of TTF-TCNQ on parylene-N is most likely to be high too. Therefore, according to these results, the terahertz devices could be produced as both model A (if silane A174 is added) and model B, and the Hall devices could be produced as model C. According to the previous scanning electron microscopy results however, the best model type for the terahertz devices is model A.

3.2 Device production

Once suitable device models had been designed, the quadratic, electrical devices were produced. All devices were produced during the same evaporation steps, eliminating the effect of structural differences between the batches. Figure 18 shows a schematic image of the terahertz devices and Hall devices produced. In order to view the surface structure and measure the exact film thicknesses deposited, another sample was also produced, a surface analysis sample. In total, five terahertz devices, five Hall devices and one surface analysis sample was produced.

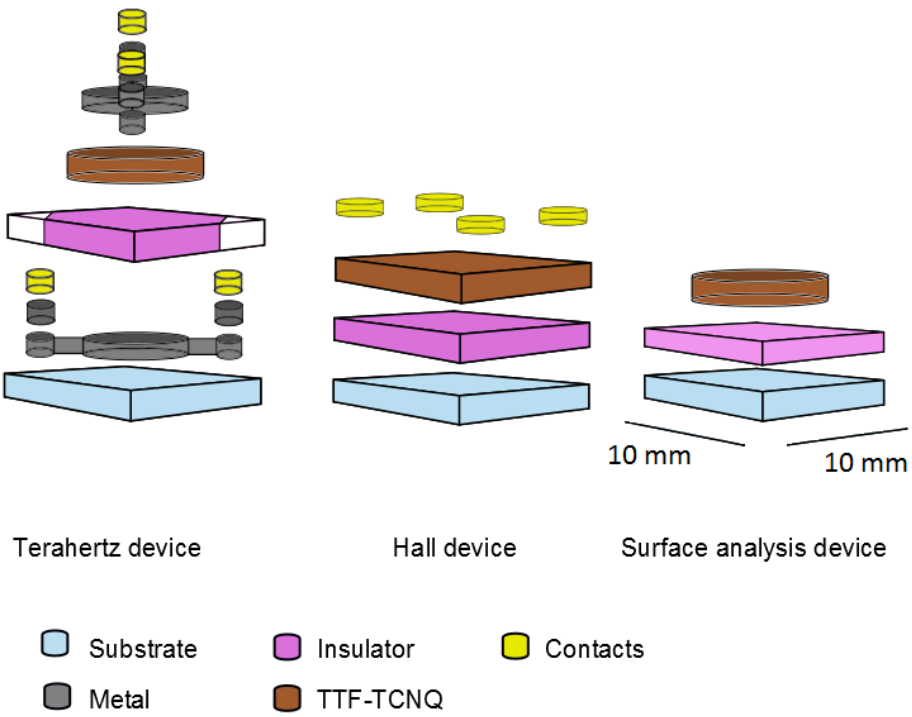

Figure 18. Design of the electrical devices and surface analysis sample produced.

Table 3 summarizes information about the different device layers for each device. Further details can be found in Appendix C about evaporation pressures and temperatures.

Table 3. Materials used for different layers in each device type.

Device	Terahertz device	Hall device	Surface analysis device
Substrate	Sapphire	Sapphire	Sapphire
Metal	Cr	-	-
Contacts	Cr + Au	Au	-
Insulator	Par-N + Sil A174	Par-N + Sil A174	Par-N + Sil A174
Sample names	THz01-05	Hall01-05	Surf01

All substrates were cleaned in the clean room according to the cleaning procedures described in Appendix A. Similar to the previous cleaning procedure, the samples were examined with a laser test in order to determine that the samples were indeed clean.

3.2.1 Layer evaporation

THz01-05 were mounted in a PVD chamber together with a chromium rod. The chamber was annealed and the pressure pumped down. After allowing the chamber to cool down, a 5 nm thick chromium film was evaporated through a mask. The samples were brought to a clean room and the mask was changed. All THz01-05 were again mounted in a PVD chamber, now together with a chromium rod and a gold boat. The pressure was pumped down whilst annealing the chamber. After allowing the chamber to cool down, a 5 nm chromium layer was deposited through the mask. Immediately after, without opening the chamber, a 15 nm gold layer was evaporated through the same mask. The film patterns and the layer sequence after these steps can be seen in Figure 19.

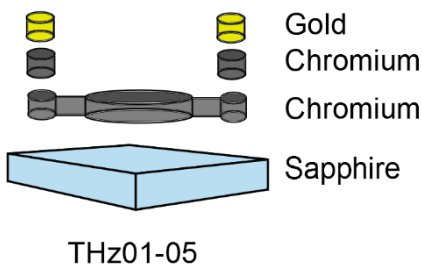

Figure 19. Schematic image of THz01-05 after evaporating chromium and gold contacts.

Following this, a homogenous insulating layer of parylene-N and silane A174 was evaporate on all samples, THz01-05, Hall01-05 and Surf01 through CVD. The thickness of the layer deposited was determined by examining the colour

of the parylene-N during the evaporation. The desired thickness was ≥ 200 nm, as this thickness creates a pin-free, insulating layer according to previous experiences. Figure 20 shows the samples after evaporating the insulator onto the samples.

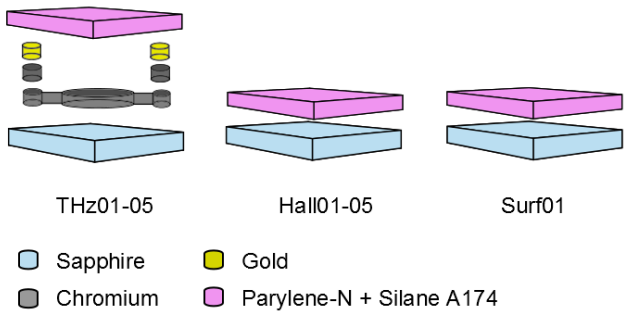

Figure 20. Schematic image of THz01-05, Hall01-05 and Surf01 after parylene-N and silane A174 evaporation.

Following this process, a Knudsen cell was cleaned and filled with TTF-TCNQ. The Knudsen cell and all samples, THz01-05, Hall01-05 and Surf01 were mounted in a PVD chamber together with the filled Knudsen cell. The pressure was pumped down whilst annealing the TTF-TCNQ. A 200 nm thick TTF-TCNQ film was evaporated through a mask on the THz01-05 and Surf01 and without a mask on Hall01-05, see Figure 21.

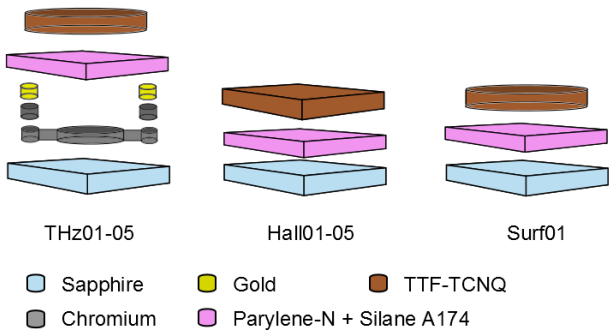

Figure 21. Schematic image of THz01-05, Hall01-05 and Surf01 after evaporating TTF-TCNQ.

All process steps for Surf01 were now completed. The final step for Hall01-05 was evaporation of gold contacts. Hall01-05 were mounted in a PVD chamber

together with a gold boat. The pressure was pumped down and a 20 nm thick gold layer was evaporated through a mask.

Subsequently, two process steps remained for the terahertz devices. THz01-05 were mounted in a PVD chamber together with a chromium rod. After pumping down the pressure, a 5 nm thick chromium layer was evaporated through a mask. The samples were taken to a clean room and the mask was changed. Again, THz01-05 were mounted in a PVD chamber, together with a chromium rod and gold boat. After pumping down the pressure a 5 nm thick chromium layer was evaporated. Immediately after this, a 20 nm gold layer was evaporated. The final structure of the terahertz devices is seen in Figure 22.

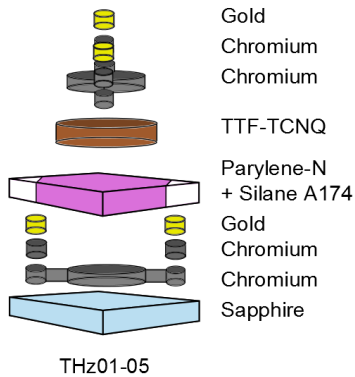

Figure 22. Schematic image of THz01-05 after evaporating chromium and gold contacts.

3.2.2 Contacting

In order to connect electrical devices to the experimental setup, electrical contacts are required. The terahertz devices and Hall devices were both contacted in a similar manner.

An electrical pin was soldered to four copper wires using soldering tin. Before connecting the wires, the copper was etched in 17 % HCl, removing any oxidized layers and dirt. The copper was dipped in Millipore water to remove any acidic residues. The same procedure was repeated for a piece of indium. Subsequently, a stray of indium was soldered onto the tip of each copper wire. The wires were then fixed to the gold contacts on the samples by simply applying pressure. An image of the contacted Hall devices can be seen in Figure 23.

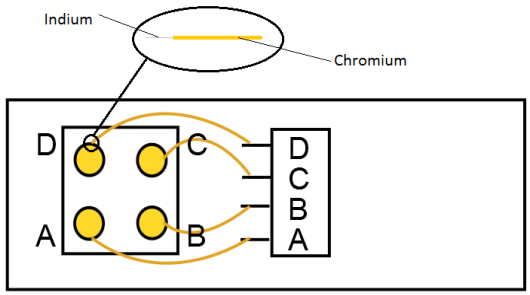

Figure 23. Schematic image of a contacted Hall device.

3.3 Device structure

Before performing any electrical measurements on the produced devices, the surface of the devices were imaged and the exact thickness of the deposited TTF-TCNQ film and parylene-N layer was measured. This imaging and measuring procedure was performed on the surface analysis sample, Surf01.

3.3.1 Surface imaging

To image the surface structure of the TTF-TCNQ layer in the electrical devices produced, images were taken on Surf01 using a scanning electron microscope. These images can be seen in Figure 24 and show a well ordered TTF-TCNQ layer deposited on parylene-N.

Both images are taken of the same sample, Surf01. It seems that a smooth surface, such as parylene-N, which is a polymer, creates a relaxed TTF-TCNQ film. The TTF-TCNQ crystallites largely follow the same direction, but sometimes change. Yet, the highly unordered surfaces due to lattice mismatch and an uneven surface as seen on chromium and glass (Figure 17) do not occur on parylene-N. An interesting further study for developing better terahertz device (and other types of devices as well) could be to investigate the TTF-TCNQ film formation on several types of homogenous polymers, both conducting and insulating.

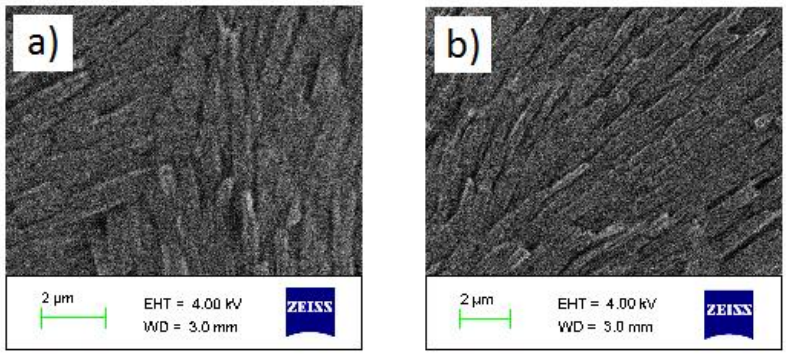

Figure 24. Surface structure of TTF-TCNQ on the electrical devices, THz01-05 and Hall01-05. The images are both taken on Surf01.

3.3.2 Film thickness

Surf01 was then used to measure the thickness of the deposited TTF-TCNQ and parylene-N layer using a profilometer. A scratch was made with a toothpick in each film and the relative height variations where recorded, producing a set of data points. These data points were used to create graphs and to calculate the film thicknesses of both TTF-TCNQ and of the insulator.

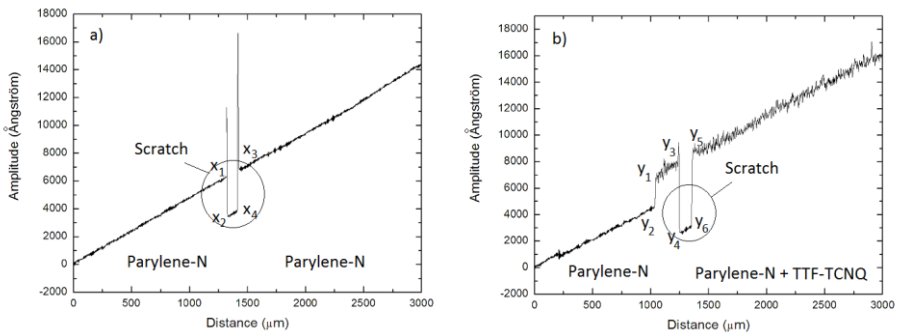

Figure 25. Graphs created from data obtained during the profilometer measurements. Graph a) shows the parylene-N thickness and graph b) the TTF-TCNQ thickness as well as the parylene-N thickness.

Figure 25 shows the graphs obtained when measuring the thickness of the deposited parylene-N film and the deposited TTF-film on parylene-N. Using this data, the exact thickness of the parylene-N and TTF-TCNQ films were calculated. The first step in Figure 25 b) shows the height of the TTF-TCNQ film. The scratch was made in both TTF-TCNQ and parylene-N and thus,

shows their combined thickness. Deducting the TTF-TCNQ from this data provides the parylene-N thickness. The scratch in Figure 25 a) was made in only parylene-N, providing data for the parylene-N thickness. The obtained value of the parylene-N film coincide well in both graphs.

Given below are the relative height values of the different points in the graphs in Figure 25 followed by the calculations for the TTF-TCNQ thickness as well as the parylene-N thickness.

$x_1 = 6320$ Å $\qquad y_2 = 4680$ Å

$x_2 = 3430$ Å $\qquad y_3 = 7810$ Å

$x_3 = 6730$ Å $\qquad y_4 = 2660$ Å

$x_4 = 3870$ Å $\qquad y_5 = 8540$ Å

$y_1 = 6730$ Å $\qquad y_6 = 3120$ Å

Calculations for the TTF-TCNQ film thickness:

$$y_1 - y_2 = 2050 \text{ Å} \approx 200\ nm$$

Calculations for the parylene-N thicknes:

From Figure 25 a):

$$\frac{(x_1 - x_2) + (x_3 - x_4)}{2} = 2875 \text{ Å} \approx 300\ nm$$

From Figure 25 b):

$$\frac{(y_3 - y_4) + (y_5 - y_6)}{2} - 2050 \text{ Å} = 3235 \text{ Å} \approx 300\ nm$$

The desired thickness of parylene-N was $\geq$ 200 nm and so, a layer of 300 nm is very good. This thickness dimension is expected to create a pin-hole free, homogenous, insulating layer, allowing the TTF-TCNQ to form a relaxed, organized film as seen in Figure 24, but yet thin enough to minimize the absorption of a terahertz radiation pulse in the insulator.

4. Hall Characterization

There are several ways of measuring the electric properties of a material. In this project, Hall characterization and terahertz measurements have been used. The concepts of these techniques are further explained in the following two chapters along with the experiments that have been performed and the results obtained.

4.1 The Hall characterization experiment

The Hall characterization is an experiment performed to determine several parameters of the charge carriers in a sample, e.g., the charge carrier concentration, the charge carrier type and the mobility of the charge carriers [29]. A voltage, V_a, is applied over a sample creating an electric field, E_x, and a current, I. A magnetic field, B_z, is applied perpendicular to E_x giving rise to a force, F_L, on the charge carriers. A schematic image of a Hall setup can be seen in Figure 26.

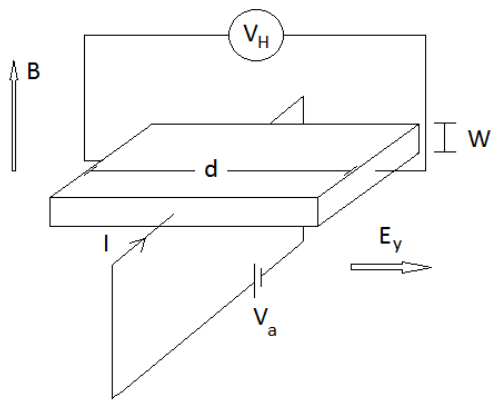

Figure 26. Circuit schematics of the Hall characterization setup.

Equation 9 describes the force resulting from the applied magnetic field, the elementary charge, and the charge carrier's velocity, v_x, in the applied electrical field's direction.

$$F_L = qv_xB_z$$

Equation 9.

This force causes an accumulation of charge carriers in one end of the sample, giving rise to a new electric field, E_y. This generated field creates a new force, F_E, counteracting the effect of F_L on the charge carrier movement.

$$F_E = qE_y$$

Equation 10.

The system eventually reaches a steady state when both forces are equally large:

$$E_y = v_xB_z$$

Equation 11.

The bias originating from the generated electric field is called the Hall voltage, V_H, and depends on the sample thickness, W as:

$$V_H = E_yd = \frac{J_xB_zd}{qn_{3D}} = \frac{IB_z}{qn_{3D}W}$$

Equation 12.

The sign of the Hall voltage depends on the type of charge carriers in the sample, and therefore indicates whether the dominating charge carriers are holes or electrons. The conductivity of the sample is found by determining the sample's resistivity, which for a quadratic sample depends only on the sample thickness and its resistance.

$$\sigma = \frac{1}{\rho} = \frac{1}{RW}$$

Equation 13.

Once the Hall voltage has been determined, the charge carrier density can be calculated. The charge carrier density together with the conductivity can be used to find the material's mobility using Equation 5.

Thus, to summarize, once the Hall voltage has been measured, the mobility, the charge carrier density and the charge carrier type can be determined [29].

4.2 Measurements

The devices used for the Hall characterization experiment, Hall01-05 are described in Chapter 3. Only two samples were successfully contacted, Hall02 and Hall05, therefore, measurements were only performed on these two samples. The circuit schematics can be seen in Figure 26. The applied voltage was set to 40 V, the current through the sample to 1 mA and the magnetic field to 0.23 T which allowed for a maximum resistance of 40 kΩ:

$$R = \frac{U}{I} = \frac{40\ V}{0.001\ A} = 40\ k\Omega.$$

Equation 14.

The sample resistance for the two devices was measured to 200 kΩ, which was above the maximum allowed resistance. Therefore, the setup was reconnected with a resistance parallel to the sample, lowering the current through the device. The value of this additional resistance was calculated as:

$$\frac{1}{R_{max}} = \frac{1}{R_{parallel}} + \frac{1}{R_{sample}} \Leftrightarrow \frac{1}{40\ k\Omega} = \frac{1}{R_{parallel}} + \frac{1}{200\ k\Omega} \Rightarrow R_{parallel} = 50\ k\Omega$$

Equation 15.

lowering the current through the sample by a factor 5.

The two successfully contacted samples, were connected to the Hall setup and the Hall voltage was measured. A computer program then calculated the conductivity, σ, resistivity, ρ, charge carrier density, n_{3D}, and mobility, μ, in each device as described in the previous section. The data obtained is summarized in Table 4. The charge carrier concentration and mobility was measured twice for each sample.

Table 4. Electric data obtained for Hall02 and Hall05.

Sample	Hall02	Hall05
$\sigma\ (S/cm)$	1.08	0.935
$\rho\ (\Omega \cdot cm)$	0.930	1.07
$n_{3D}\ (cm^{-3})$	$3.74 \cdot 10^{18}$	$4.36 \cdot 10^{18}$
$n_{3D}\ (cm^{-3})$	$3.14 \cdot 10^{18}$	$5.32 \cdot 10^{18}$
$\mu\ (cm^2/Vs)$	2.050	1.345
$\mu\ (cm^2/Vs)$	2.210	1.095

As explained above, the conductivity and resistivity are characteristic for a material. Both samples have a resistivity and conductivity around 1 S/cm. This coincides well with the resistivity along the a-direction of the unit cell measured by another research group. This group used single crystalline TTF-TCNQ, enabling electrical characterization in each lattice dimension. They found that σ_b = 400 S/cm, σ_c = 5 S/cm and σ_a = 0.5 S/cm at room temperature [17]. In this project, polycrystalline TTF-TCNQ was used. As TTF-TCNQ is highly anisotropic, single crystalline TTF-TCNQ will provide higher electric conductivity results in the highest conducting lattice direction, as the properties are measured in only one dimension. Measuring the conductivity of an anisotropic polycrystalline film will cause much lower conductivity values as the charge carrier conduction will be due the short, non-linked rods of TTF-TCNQ. The charge carrier's paths are also limited by impurities and defects as previously discussed. Hence, if the sample is of poor quality, the values will be low as well.

The measured Hall voltage was positive, indicating that an applied magnetic field over the device accumulates holes (if the voltage would have been negative, the accumulated carriers would have been electrons). This mean that the dominating charge carriers are holes, which in turn means that the conductivity is dominated by the TTF chains. The relation between the measured Hall voltage and the charge carrier concentration can be seen in Equation 12. A high Hall voltage indicates a low charge carrier concentration and a low Hall voltage indicates a high charge carrier concentration. As TTF-TCNQ is both electron and hole conducting, the created field providing the Hall voltage might be very low due to both electron and hole accumulation in each end of the device. This in turn would therefore misguidingly be interpreted as a high charge carrier concentration value in our analysis, which may not be the actual free charge carrier concentration. However, the Hall analysis used requires that there should be only one dominating charge carrier, and so, the values for the charge carrier concentration for TTF-TCNQ are uncertain.

A higher charge carrier concentration will according to Equation 5 provide a lower mobility. Therefore, the mobility values obtained are also uncertain and are most likely higher than the ones recorded. A researcher in 1977 calculated the mobility of TTF-TCNQ at room temperature as 3 cm^2/Vs [31]. This value is higher than what was recoded here, further indicating that the device produced here are poor conductors. Furthermore, it is not necessary that the mobilities for holes and electrons in TTF-TCNQ are equally large. Even though the Hall voltage indicates holes as the dominating charge carrier, this in fact merely indicates that the hole mobility may be larger than the electron mobility. Nevertheless, this as well cannot be determined from these experiments.

To further examine the samples through Hall measurements, the Hall voltage could be measured as a function of the magnetic field. A higher magnetic field causes a larger charge carrier accumulation and hence, a greater Hall voltage. Measuring the properties at different magnetic fields would give a better certainty in the obtained results. Nevertheless, as there is not only one dominating charge carrier in TTF-TCNQ, such measurements would most likely not give accurate charge carrier concentrations. So, to conclude, the values obtained during these measurements are not reliable.

5. Terahertz characterization

5.1 The terahertz characterization experiment

The basic principle of terahertz spectroscopy is to send a pulse of radiation through a thin film and to measure how much is transmitted. The outgoing transmission signal depends on the number of charge carriers able to interact with the radiation pulse, and their mobility. A schematic image of a terahertz setup can be seen in Figure 27.

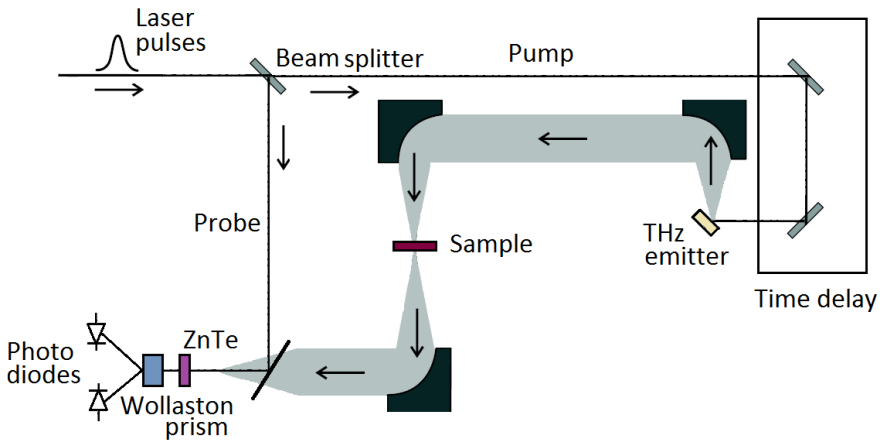

Figure 27. Schematic image of a terahertz spectroscopy setup. The generated laser pump is split in two beams, the probe and the pump. One beam (the pump) is time-delayed and shot through the sample. The transmission signal and probe signal are merged together again and time resolved by electro optic sampling.

In this project, 80 fs electromagnetic light pulses are generated by a laser with wavelength 780 nm and repetition frequency 80 MHz. The laser pulse is split in two beams, the probe and the pump. The pump is time delayed and generates pulses of terahertz radiation in the picosecond range after excitation of a terahertz emitter [31, 32].

The terahertz emitter consists of a semiconductor. As a pulse hits the emitter the light absorption causes charge carrier excitations, creating electron-hole pairs. The generated carriers are accelerated in an applied electric field, separating the negatively charged electrons and positively charged holes. This charge separation creates a polarization which, in turn, creates a transient current which causes emission of terahertz radiation at a frequency around 2 THz [32, 33, 34]. A graphical display of what happens in the terahertz emitter can be seen in Figure 28.

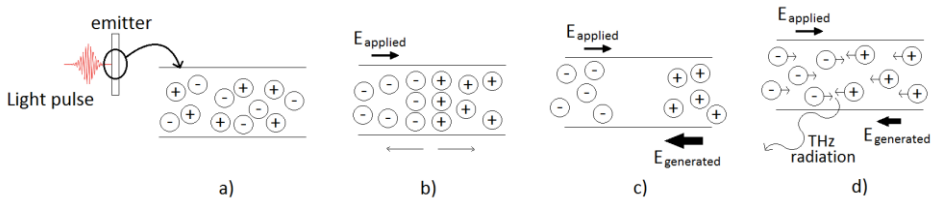

Figure 28. Generation of a terahertz pulse. As the laser pulse hits the emitter, electron-hole pairs are generated through excitation (a). An applied electric field accelerates the charge carriers (b), creating a dipole moment, generating a transient electric field (c). This charge carrier oscillation causes the emission of terahertz radiation (d).

The terahertz pulse is focused and shot through the sample and then remerged with the probe signal. Following this, the transmission signal and probe signal are time-resolved by electro-optic sampling in a ZnTe crystal. The slowly oscillating, long transmitted terahertz pulse (the pump) acts as an applied bias over the short laser pulse (the probe), causing the polarization of the laser pulse to rotate in the ZnTe crystal. This rotation is proportional to the terahertz pulse's electric field, which depends on the pulse's interaction with the charge carriers in the sample and thus the material's electrical properties. Due to different polarizations, the beam is split up once again in a Wollaston prism whereafter, each contribution is measured by photodiodes. The generated terahertz signal is the difference between these two photocurrents. The transmission signal is affected by all device layers, hence, it is important to produce a device that minimizes the absorption of the signal in other parts of the sample than the layer to be examined [31, 32, 33].

In order to only examine the electric properties of the thin film, the charge carrier sheet density, n_{2D}, which is the number of charges per unit area, is altered by applying an external electric field over it as seen in Figure 29. As the sheet carrier density is altered, the number of mobile charge carriers able to interact with the incoming terahertz radiation is altered and thus, changes the transmission signal. Comparing the transmission signal with and without an applied bias therefore, provides the true signal for the thin film material. As a bias is applied over the material of interest, charge carriers can both be

injected or depleted depending on the bias direction and the charge carrier type in the sample. Figure 29 shows schematic images of what happens as a negative and positive bias is applied on both a n-type material, where the dominating charge carriers are electrons, and on a p-type material, where the dominating charge carriers are holes.

The capacitance, C, in a material is a measure of how well a material can store electric charge. The capacitance is measured as charge per unit voltage. A change in the capacitance by an applied voltage changes the sheet carrier density. Equation 16 shows how a change in bias changes the sheet carrier density.

$$\Delta n_{2D} = \frac{C}{eA}\Delta V$$

Equation 16.

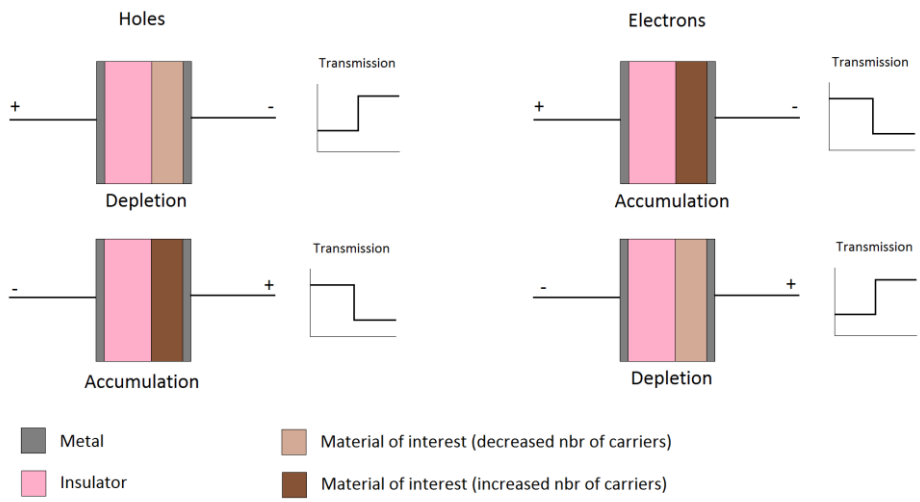

Figure 29. Schematic image of what occurs when a bias is applied over a material, showing the charge carrier injecting and depletion for both holes and electrons and how this changes the transmission signal.

If the applied bias causes an accumulation of charge carriers (either holes or electrons) in the sample, the transmission signal decreases as the number of carriers able to interact with the terahertz pulse increases. If the applied bias instead causes a depletion of charge carriers in the sample, the transmission signal increases as the number of charge carriers able to interact with the pulse decreases. Figure 30 shows a graph of an earlier recorded transmission signal during electromodulation (not in TTF-TCNQ) [31].

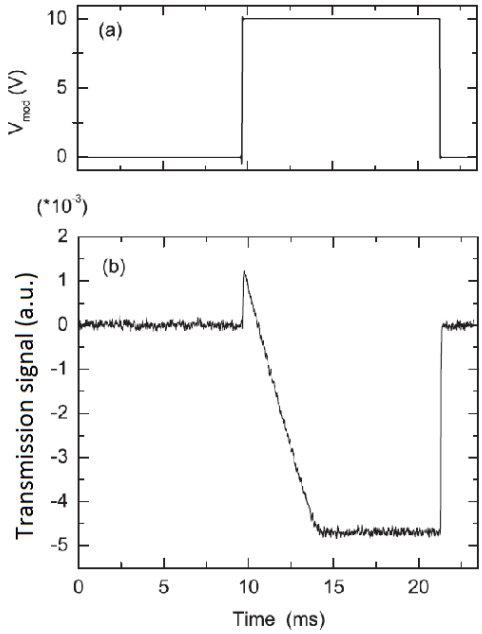

Figure 30. A recorded transmission signal where a bias is applied after 10 ms. The applied bias causes a change in the number of charge carriers able to interact with the incoming terahertz pulse [31].

No voltage is applied at first, after 10 ms the sample is electromodulated by applying a bias of 10 V. After around 22 ms the bias is removed, restoring the sample's original sheet carrier density. As a bias is applied, the charge carrier density can be either increased or decreased depending on the dominating carrier type as explained above. An increased density increases the number of charge carriers able to interact with the incoming terahertz pulse and thus, reduces the electric field of the transmission signal. In Figure 29 the transmission signal decreases as the bias is applied, indicating an increased sheet carrier density through excitation. As the bias is removed, the excited charge carriers recombined into a steady state again [31].

From this data, the conductivity $\Delta\sigma_{2D}$, of the material can be calculated according to Equation 17 [35]:

$$S = \frac{E(t) - E_{no\ bias}}{E_{no\ bias}} = \frac{-Z}{2n}\Delta\sigma_{2D}$$

Equation 17.

where S is the transmission signal, $E(t)$ is the electric field of the transmitted pulse as a function of time, n is the refreactive index and Z is the impedance in vacuum.

To be able to apply a bias over the thin film it must be embedded between two metal contacts and an insulator. To prevent a current breakthrough through the insulator, current-voltage-(IV)-measurements should be performed prior to terahertz measurements in order to find a suitable bias for the electromodulation.

5.2 IV-measurements

Before performing terahertz spectroscopy on a terahertz devices, the suitable voltage for electromodulation has to be determined. A too high voltage may cause a current breakthrough through the insulator, which is highly unwanted as it would destroy the device. Therefore, IV-measurements must first be performed.

The circuit scheme for an IV-setup can be seen in Figure 31. In this project, the maximum current was set to 10 nA and the IV-characteristics where measured several times in both bias directions up to +10 V and down to -10 V. There was only one successfully produced and contacted sample, THz02, therefore, measurements were only performed on this sample.

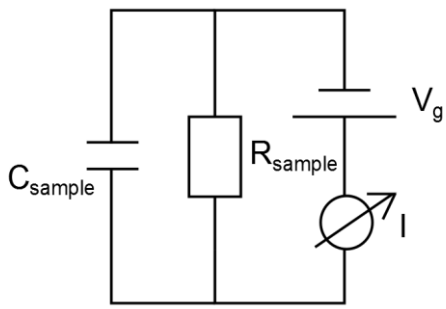

Figure 31. Circuit schematics of the IV-measurement setup.

The recorded results from the IV -measurements are seen in Figure 32.

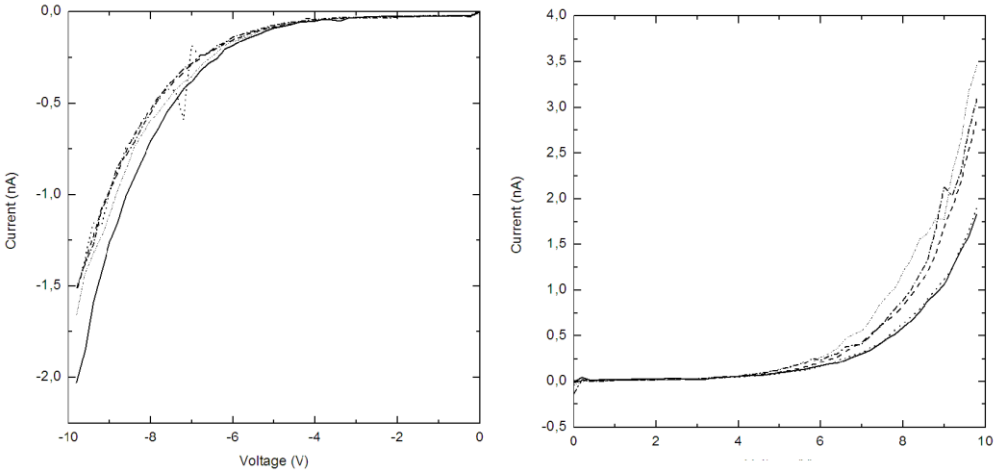

Figure 32. Repeated IV-measurements of the terahertz sample, THz02, in both gate bias directions.

The IV-curves are more consistent for the negative bias than for the positive bias. Therefore, a negative bias of -10 V will be used to electromodulate the sample. The low leakage current for this voltage indicates a good insulating parylene-N film.

The capacitance of the sample was also measured in order to calculate the injected sheet carrier density according to Equation 16. To avoid contributions from the cable's capacitance, this was also measured and deducted from the measured sample capacitance:

Applied voltage, $\Delta V = 10\ V$

Area of TTF-TCNQ film, $A = 28\ mm^2$

Measured sample capacitance, $C_{sample} = 1.38\ nF$

Measured cable capacitance, $C_{cable} = 0.18\ nF$

True sample capacitance of the sample:

$$C = C_{sample} - C_{cable} = 1.38\ nF - 0.18\ nF = 1.20\ nF$$

Sheet carrier density, calculated using Equation 16:

$$\Delta n_{2D} = \frac{C}{eA}\Delta V = \frac{1.20 \cdot 10^{-9}\ F}{e \cdot 0.28\ cm^2} \cdot 10\ V\ \approx 2.67 \cdot 10^{11} cm^{-2}$$

This sheet carrier density shows the change in the amount of charge carriers interacting with the incoming terahertz pulse during terahertz spectroscopy

when an electromodulating bias of 10 V is applied. This change in charge carrier density changes the outgoing transmission signal as shown in Figure 29 and thus the recorded terahertz signal.

5.3 Terahertz measurements

Once a suitable voltage had been determined through *IV*-measurements, terahertz spectroscopy was performed on THz02 using the setup seen in Figure 27. The sample was kept at room temperature in vacuum at a pressure of 0.39 mbar. The laser used had a wavelength of 780 nm, creating terahertz pulses with frequencies around 0.2-2.7 THz. The electromodulating bias was set to -10 V and was triggered after half the recording time. Figure 33 shows the graph obtained:

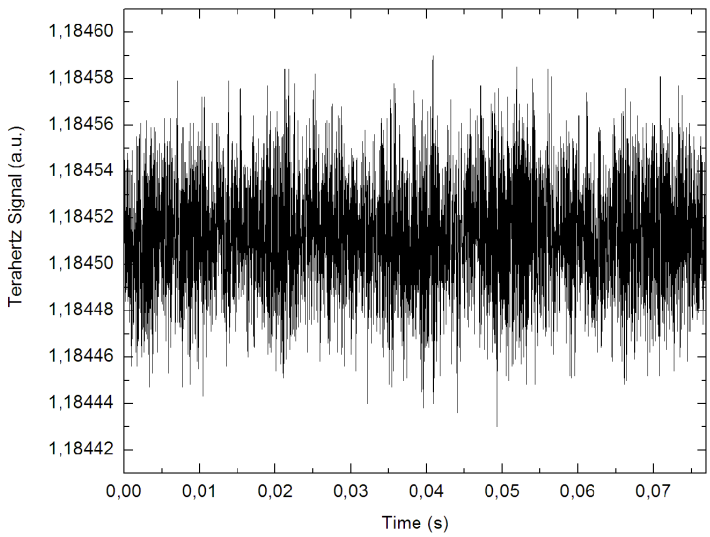

Figure 33. Recorded terahertz signal of THz02. After half the recorded time the sample was electromodulated by a bias of -10 V.

The terahertz signal is defined as the difference between the two photocurrents of the probe and pump beam relative the probe. After half the measuring time a voltage of -10 V is applied over the sample causing an electromodulation, changing the number of charge carriers possible to interact with the incoming terahertz pulse. This change in the charge carrier density should show a

change in the transmission signal in form of a step function as seen in Figure 29. However, no such step is observed in Figure 33. TTF-TCNQ has a high conductivity [8], and a step function should be observed. However, if the quality of the sample produced here is very poor, the long range order providing charge transfer along the molecular chains may be disturbed by defects and impurities, rendering the device an insulator. Applying a higher bias could enable charge carriers to hop between energy states, however, this may also cause a breakthrough of the current through the insulator, destroying the device. These results coincide well with those obtained during the Hall characterization experiment, which indicated that the samples produced were poor conductors. Another reason for why no step is observed may be that there are an equal amount of holes accumulated as there are electrons depleted. As seen in Figure 29 an accumulation of holes causes an increase of charge carriers able to interact with the incoming terahertz pulse, reducing the transmission signal. A depletion of electron causes a decrease of charge carriers able to interact with the pulse, increasing the transmission signal. Therefore, an equal amount of charge carriers being depleted and accumulated will cancel out the change in transmission and nothing will be observed in the terahertz graph.

6. Conclusion

TTF-TCNQ as the material of interest have been produced and examined.

Terahertz devices require the ability of applying a bias over the material to be examined. It must therefore, be embedded between two metals and an insulator. The adhesion strength of TTF-TCNQ was high on all underlying substrates. The adhesive strength on parylene-N could however not be determined due to the poor adhesive skills of parylene-N itself causing all parylene-N to be removed during the test. Nevertheless, due to the overall high adhesion strength of TTF-TCNQ it was presumed to adhere well to parylene-N too. To increase the adherence of parylene-N to its underlying substrate, silane A174 was incorporated in the CVD process of the insulating film. The surface structure of TTF-TCNQ on both a metal, chromium, and an insulator, parylene-N was imaged using a scanning electron microscope. The most ordered and relaxed surface occurred on the parylene-N polymer. Parylene-N forms a homogenous smooth surface, enabling deposition of a smooth, ordered layer. The interface between TTF-TCNQ and chromium may produce an energy costing lattice strain [27] creating a disordered TTF-TCNQ film. The Hall devices can be produced with the material of interest directly on the substrate, e.g. glass. However, the porous structure of glass also produces a highly disordered film. Therefore, all Hall devices were also produced with an underlying parylene-N film beneath the TTF-TCNQ layer.

The electrical properties obtained from the Hall characterization measurements and terahertz measurements indicated that the devices produced where of poor quality. The charge carrier concentration measured during the Hall experiment was high, however, the conductivity was very low indicating a low mobility. The reason for this may be poor π-bond overlaps or poor device qualities with many defects, disrupting the electrical conduction along the molecular chains. As TTF-TCNQ is both electron and hole conducting, the accumulation of holes causes a lower Hall voltage. Therefore, the charge carrier concentration obtained may not be the actual charge carrier concentration due to an “incorrect” Hall voltage, meaning that the mobility of the devices most likely are higher than the values obtained. No information could be obtained from the terahertz spectroscopy experiment as no change in transmission was observed during electromodulation. This may be caused by

an equal amount of holes being accumulated and electron being depleted, causing the change in transmission to be cancelled out as TTF-TCNQ is both electron and hole conducting.

Despite the low values of the mobility and conductivity of TTF-TCNQ obtained during these experiments, the benefits of a highly conducting organic material are large, especially within organic electronics. TTF-TCNQ is proven to indeed have a high conductivity along one dimension [8]. Using polycrystalline films, as done in this project, is not beneficial if a high conduction is desired as the charge carrier transport is highly anisotropic and will be limited by the lowest conduction direction. Moreover, polycrystalline materials require charge carriers to be transported across grain boundaries, decreasing the speed of charge transport further. As the availability of inorganic metals decrease, the importance of synthetic organic materials with high conductivity increase. As research progresses, so will the number of applications using TTF-TCNQ as an active material. Thus, not only will the economic costs decrease as these types of materials transit into industries but also the ecological effects, creating a more sustainable development.

There were several limitations of this project due to the restricted time period and machinery available. Nonetheless, this project has given a good overview of many different types of laboratory work and research methods. The project has significantly increased the ability to work both independently and in group and to organize and structure larger scale scientific research and projects in an efficient and productive manner.

References

[1] Norgate, T. E., Jahanshahi, S., Rankin, W. J., (2007) Assessing the environmental impact of metal production processes. *J. Clean. Prod.* 15 (8/9) p. 838-848.

[2] Nriagu, J. O. (1988) A Silent Epidemic of Environmental Metal Poisoning? *Environ. Pollut.* 50 (1-2) p. 139-161.

[3] Smil, V. (2003) *The Earth's Biosphere: evolution, dynamics, and change.* Massachusetts: MIT.

[4] Mukherjee, B., Mukherjee, M. (2011) High Performance Organic Thin Film Transistors with Solution Processed TTF-TCNQ Charge Transfer Salt as Electrodes. *Langmuir.* 27 (17) p. 11246-11250.

[5] Pauliukaite, R., Malinauskas, A., Zhylylak, G., Spichiger-Keller, U. E. (2007) Conductive Organic Complex Salt TTF-TCNQ as a Mediator for Biosensors. An Overview. *Electroanal.* 19 (24) p. 2491-2498.

[6] Odom, S., *et. al.* (2010) Restoration of Conductivity with TTF-TCNQ Charge Transfer Salts. *Adv. Funct. Mat.* 20 (11) p. 1721-1727.

[7] Davies, J. H. (2006) *The Physics of Low-Dimensional Semiconductors: An Introduction.* 6th ed. New York: Cambridge University Press.

[8] Kasap, S., Copper, P. (2006) *Springer Handbook of Electronic and Photonic Materials.* Würtzberg: Springer.

[9] Inagaki, S. (2009) *Orbitals in Chemistry.* Heidelberg: Springer.

[10] Grossmann, G. (2008) *Elektroniska material.* Lund: Fasta Tillståndets Fysik.

[11] Askeland, D. R. and Fulay, P. P. (2010) *Essentials of Materials Science and Engineering.* 2nd ed. Canada: Cengage Learning.

[12] Bao, Z., Locklin, J. (2007) *Organic Field-Effect Transistors.* Florida: Taylor & Francis Group.

[13] Koch, N., Ueno. N, Wee, A. T. S. (2013) *The Molecule-Metal Interface.* Weinheim: Wiley-VCH.

[14] Grundmann, M. (2010) *The Physics of Semiconductors*. 2nd ed. Heidelberg: Springer.

[15] Blundy, J. and Wood, B. (2003) Partitioning of trace elements between crystals and melts. *Earth. Planet. Sci. Lett*. 10 (3-4) p. 383-397.

[16] Solovyeva, V. (2011) *TTF/TCNQ-based thin films and microcrystals - growth and charge transport phenomena*. Dissertation. Johann Wolfgang Goethe Universität: Frankfurt am Main.

[17] Beltrán, J.L., Flores, F., Martinez, J. L., Ortega, J. (2013) Energy Level Alignment in Organic-Organic Heterojunctions: The TTF/TCNQ Interface. *J. Phys. Chem. C*. 117 (8) p. 3888-3894.

[18] Tafra, E., Culo, M., Basletic, M., Korin-Hamzic, B., Hamizic A., Jacobsen, C. S. (2012) The Hall effect in the organic conductor TTF-TCNQ: choice of geometry for accurate measurements of a highly anisotropic system. *J. Phys. Condens. Matter*. 24 (4) p. 1-6.

[19] Chiang, C. K., Cohen, M. J., Newman, P. R., Heeger, A. J. (1977) Effect of controlled disorder on the electrical properties of TTF-TCNQ (tetrathiafulvalene-tetracyanoquinodimethane): High-temperature regime. *Phys. Rev. B*. 16 (12) p. 5163-5172.

[20] Kakani, S. L. and Kakani, A. (2004) *Material Science*. New Dehli: New Age International Publishers.

[21] Tan, C. P., Craighead, H. G. (2010) Surface Engineering and Patterning Using Parylene for Biological Applications. *Mater*. 3 (3) p. 1803-1832.

[22] Yeh, P. (1988) *Optical Waves in layered media*. New York: John Wiley & Sons.

[23] Fortin, J. B. and Lu, T.-M. (2004) *Chemical Vapor Deposition Polymerization - The growth and properties of Parylene thin films*. Boston: Kluwer Academic Publisher.

[24] Mattox, D. M. (2010) *Handbook of Physical Vapor Deposition (PVD) Processing*. 2nd ed. Burlington: Elsevier Inc.

[25] Chambers, A., Fitch, R. K., Halliday, B. S. (1998) *Basic Vacuum Technology*. 2nd ed. Bristol: Institute of Physics Publishing.

[26] Harsha, K. S. S. (2006) *Principles of Vapor Deposition of Thin Films*. Oxford: Elsevier Ltd.

[27] Le Bourhis, E. (2008) *Glass: Mechanics and Technology*. Weinheim: Wiley-VCH.

[28] Verma, N. K. (2014) *Physics for Engineers*. New Dehli: PHI.

[29] ASTM Standard D3359, 1997, *Standard Test Methods for Measuring Adhesion by Tape Test*, ASTM International, West Conshohocken, PA, 1997, DOI: 10.1520/D3359-97, www.astm.org.

[30] Sze, S. M. and Ng, K. K. (2007) *Physics of Semiconductor Devices*. 3rd ed. New Jersey: John Wiley & Sons.

[31] Conwell, E. M. (1977) Mobility in Tetrathiafulvalene-Tetracyanoquinodimethane (TTF-TCNQ). *Phys. Rev. Let.* 39 (12) p. 777-780.

[32] Engelbrecht, S. G., Reichel, A. J, Kersting, R. (2012) Charge carrier relaxation and effective masses in silicon probed by terahertz spectroscopy. *J. Appl. Phys.* 112 (12) p. 1-6.

[33] Kersting, R., Chen, H.-T., Karpowich, N., Cho, G. C. (2004) Terahertz microscopy with submicrometre resolution. *J. Opt. A: Pure Appl. Opt.* 7 (2) p. S184-S189.

[34] Dexheimer, S. L. (2008) *Terahertz Spectroscopy: Principles and Applications*. Florida: Taylor and Francis Group.

[35] Chen, H.-T. and Kersting, R. (2003) Terahertz imaging with nanometer resolution. *Appl. Phys. Let.* 83 (15) p. 3009-3011.

[36] Engelbrecht, S.G., De Angelis, L., Tönnies, M., Kersting, R. (2013) Electronic response in mesoscopically disordered zinc oxide probed by terahertz spectroscopy. *Appl. Phys. A.* 113 (3) p. 641-644.

Appendix A *Cleaning process*

The entire cleaning process takes place in a clean room, mainly on a wet bench. Any utensils used are cleaned with acetone and isopropanol prior to utilization before every process step.

All substrates are cleaned using the same procedure. A series of ultrasonic baths (UB) are involved in the cleaning process, the chemicals used and their settings for temperature, T, and time, t, are listed in the table below.

Table A1. UB data for the chemicals used during substrate cleaning.

Chemical	t (min)	T (℃)
MIBK Methyl isobutyl ketone	5	20
IPA Isopropanol	5	20
1 % Hellmanex	45	40
MP Millipore water	5	20

The cleaning procedure is as follows:

1. Place the substrates in an UB in MIBK.
2. Place the substrates in an UB in IPA.
3. Dry the substrates with N_2-gas and place in new holder.
4. Place the substrates in an UB in 1 % Hellmanex.
5. Rinse the substrates in two beakers of MP water.
6. Etch the substrates in Piranha acid (5 parts 95 % H_2SO_4, 2 parts 30 % H_2O_2) on a hot plate, $T = 150℃, t = 60\ min$.
7. Rinse the substrates in three beakers of MP water.
8. Place the substrates in an UB in MP water.
9. Dry the substrates with N_2-gas and place in a new holder.
10. Etch the substrate in 1:1:3 solution (1 part 32 % HCl, 1 part 30 % H_2O_2, 3 parts MP water) on a hot plate, $T = 120℃, t = 15\ min$.
11. Rinse the substrates in a beaker of MP water.

12. Place the substrates in an UB in MP water.
13. Place the substrates in an UB in IPA.
14. Dry the substrates with N_2-gas and place in a plasma etcher.
15. Plasma etch samples with O_2-gas for $t = 6\ min$.

Appendix B *Device design*

The samples produced for defining a suitable device design underwent a series of evaporations. The details for these procedures are listed in the table below. The masks used for evaporating different patterns are shown in figure B1.

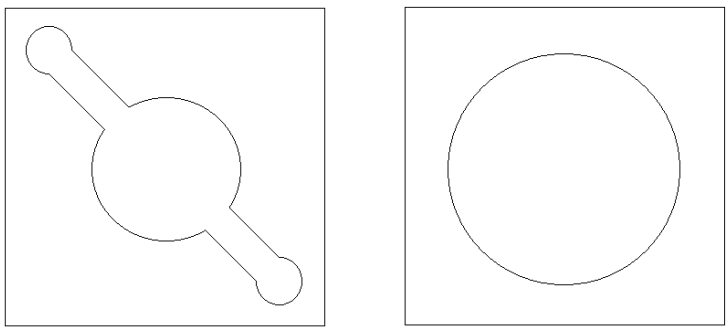

Figure B1. Different masks used during PVD.

Table B1. Evaporation data over each deposited layer during device design.

Material	Cr	TTF-TCNQ
Mask	Butterfly	Round
Pressure ($mbar$)	$8.4 \cdot 10^{-8}$	$6.8 \cdot 10^{-7}$
Annealing temperature	80℃	65℃
Type of heating	Resistive	Lamp, $110 - 170$℃
Evaporation rate	$0.5 - 0.7$ Å$/s$	$0.03 - 1.4$ Å$/s$
Film thickness	5 nm	150 nm
Sample temperature	23℃	23℃

Appendix C *Device production*

The device production contains many evaporation processes. All devices were produced during the same evaporation procedures, but the data has been broken down into tables over each device type for convenience. Figure C1 shows the different types of masks used during PVD.

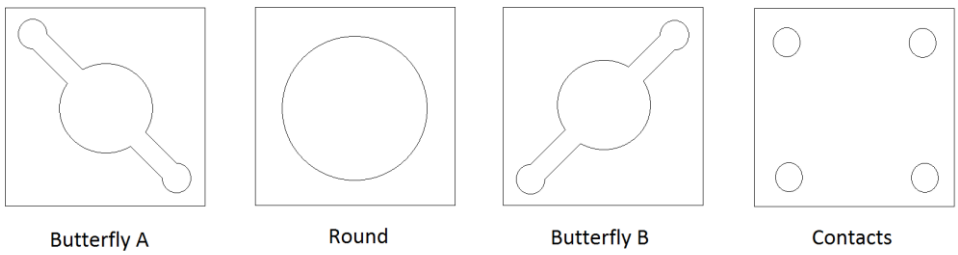

Figure C1. Different masks used during the PVD processes involved in the device production.

The material in the tables below are listed from left to right as the layer sequence starting with the substrate and going up.

Table C1. Evaporation data for THz01-05.

Material	Cr	Cr	Au	TTF-TCNQ	Cr	Cr	Au
Mask	Butterfly A	Contacts	Contacts	Round	Butterfly B	Contacts	Contacts
Pressure $(mbar)$	$3.0 \cdot 10^{-7}$	$1.8 \cdot 10^{-7}$	$3.4 \cdot 10^{-6}$	$2.6 \cdot 10^{-7}$	$1.5 \cdot 10^{-7}$	$2.3 \cdot 10^{-6}$	$4.4 \cdot 10^{-6}$
Annealing temperature	80℃	80℃	80℃	65℃	-	-	-
Type of heating	Resistive	Resistive	Resistive	Lamp $182 - 189$ ℃	Resistive	Resistive	Resistive
Evaporation rate $(Å/s)$	0.5	0.5	0.5	$0.3 - 0.4$	0.5	0.5	0.5
Film thickness	5 nm	5 nm	15 nm	200 nm	5 nm	5 nm	20 nm
Sample temperature	23℃	23℃	23℃	23℃	23℃	23℃	23℃

Table C2. Evaporation data for Hall01-05.

Material	TTF-TCNQ	Au
Mask	Round	Contacts
Pressure $(mbar)$	$2.6 \cdot 10^{-7}$	$2.3 \cdot 10^{-6}$
Annealing temperature	65℃	-
Type of heating	Lamp	Resistive
Evaporation rate $(Å/s)$	$0.3 - 0.4$	0.5
Film thickness	200 nm	20 nm
Sample temperature	23℃	23℃

Table C3. Evaporation data for Surf01.

Material	TTF-TCNQ
Mask	Round
Pressure	$2.6 \cdot 10^{-7}$
Annealing temperature	65℃
Type of heating	Lamp
Evaporation rate	$0.3 - 0.4$
Film thickness	200 nm
Sample temperature	23℃